

UNIVERSITY MEDICAL CENTER HAMBURG-EPPENDORF

Institute of Experimental Pharmacology and Toxicology
Center for Experimental Medicine
Director: Prof. Dr. Thomas Eschenhagen

The unfolded protein response in *Mybpc3*-targeted mice with hypertrophic cardiomyopathy

Dissertation

submitted to the
Faculty of Medicine
University of Hamburg
for the degree
Doctor of Medicine

by

Markus Sauer
from Kassel

Hamburg 2011

Accepted by the Medical Faculty of the University of Hamburg at: December 7th, 2012

Published with the consent of the Medical Faculty of the University of Hamburg

Examination board: Chairperson: Prof. Dr. L. Carrier

Examination board: 2. Referee: PD H.-J. Kreienkamp

Examination board: 3. Referee: Prof. Dr. M. Glatzel

Table of contents

Table of contents	I
1 Introduction	1
1.1 Hypertrophic cardiomyopathy	1
1.2 Mutations in cardiac myosin-binding protein C gene	3
1.3 Disturbances of protein degradation in hypertrophic cardiomyopathy	5
1.4 Endoplasmic reticulum stress and the unfolded protein response	6
1.5 The unfolded protein response as cause of disease	9
1.6 Aim of the thesis	11
2 Material and Methods	12
2.1 Material	12
2.1.1 Animals	12
2.1.2 Chemicals	14
2.1.3 Chemicals with risk (R-) and safety (S-) phrases	16
2.1.4 Antibodies	17
2.1.5 Kits	18
2.1.6 Oligonucleotides	18
2.1.7 Consumable Materials	18
2.1.8 Laboratory Equipment	19
2.2 Methods	21
2.2.1 Organ extraction	21
2.2.2 RNA analysis	21
2.2.3 Protein analysis	24
2.2.4 Cell culture analysis	27
2.2.5 Statistical analysis	28
3 Results	29
3.1 Evaluation of cardiac hypertrophy	29
3.2 Evaluation of protein degradation	30
3.2.1 Determination of Ub ^{G76V} -GFP protein levels	30
3.2.2 Determination of Ub ^{G76V} -GFP mRNA levels	32
3.2.3 Evaluation of the chymotrypsin-like activity	32
3.2.4 Summary	33
3.3 Evaluation of the unfolded protein response in KO and KI mice	34
3.3.1 Qualitative PCR analysis	34
3.3.2 Evaluation of the UPR trigger GRP78	34
3.3.3 Evaluation of the IRE1 α pathway	37
3.3.4 Evaluation of the ATF6 pathway: CHOP and Bcl-2 mRNA levels	40

3.3.5	Evaluation of the PERK pathway	40
3.3.6	Evaluation of chaperones' induction	42
3.3.7	Determination of oxidative stress antagonist Metallothionein-1	43
3.3.8	Evaluation of GRP78, CHOP and ATF4 at different time points in KI	43
3.3.9	Summary	45
3.4	The unfolded protein response in neonatal mouse cardiomyocytes	46
3.4.1	Analysis of GRP78, XBP-1 and CHOP in KI and WT NMCM	46
3.4.2	Treatment of NMCM with UPR inducers tunicamycin and thapsigargin	47
3.4.3	Summary	51
4	Discussion	52
4.1	Impairment of the ubiquitin-proteasome system in <i>Mybpc3</i> -KI mice	52
4.2	Decreased UPR in <i>Mybpc3</i> -KI mice	53
4.3	Increased UPR in <i>Mybpc3</i> -KO mice	55
4.4	Impact of UPR alterations on HCM and outlook	55
4.5	Clinical relevance and concluding remarks	57
5	Abstract	59
6	Deutsche Zusammenfassung	60
7	Literature	61
8	Appendix	66
8.1	List of abbreviations	66
8.2	Curriculum vitae	70
8.3	Declaration	71
8.4	Acknowledgement	72

1 Introduction

In cases of hypertrophic cardiomyopathy, the human heart tends to grow until dysfunction is inevitable. This investigation focuses on the involvement of the unfolded protein response, a cellular defense strategy, in this clinical picture.

1.1 Hypertrophic cardiomyopathy

The heart is a muscular pump that collects blood from all tissues and redistributes it after oxygenation within the lungs. Its internal anatomy reveals a system of four chambers of myocardium connected in-line. The upper ones (atria) mainly serve as collecting chambers, while the lower ones (ventricles) are stronger muscles which ensure the main pumping mechanism. The right atrium and ventricle collect blood from the periphery and forward it to the pulmonary circulation. After oxygenation, blood enters the left atrium and returns to systemic circulation by the left ventricle. The one-way flow of blood through the heart is maintained by a set of four valves. Two, which avoid reflux from the atria to the adducting vessels and another two, which avoid back current from the ventricles to the atria. Ventricles and atria are respectively separated by a muscle wall, the septum.

In hearts suffering from hypertrophic cardiomyopathy (HCM) in many cases the cells of this interventricular septum *expand* and hereby obstruct the ventricular outflow (for review, see Bonne et al., 1998; Figure 1.1). This increased flow resistance again causes left ventricular hypertrophy (LVH), especially of the left ventricle's lateral wall. Hereby a vicious circle can be established which is considered as one major determinant of this disease (for review, see Sherrid, 2006).

Hypertrophic cardiomyopathy is the most common *inherited* cardiac disorder. Its prevalence is 1:500 in the general population of industrial countries (Maron et al., 1995). The clinical appearance of HCM is very variable which might be attributable to the heterogeneity of the causing genes, which will be explained later on. Symptoms as dyspnea, occasionally orthopnea, general fatigue or even pectoral angina may or may not be observed at any age. The individual patient's clinical course varies from sudden cardiac death during adolescence to chronic heart failure in old-age (Maron, 2002).

Morphologic investigations of patients' hearts revealed the major determinants of the disease. Left ventricular hypertrophy without any other causing condition is defined as the morphological key feature of HCM, which can be well assessed by echocardiography (for review, see Seidman et al., 2001). The location of the abnormal hypertrophy is most often the anterior septum, although it can occur in any segment. As explained earlier, left ventricular outflow obstruction is considered as one of the main determinants of HCM's pathophysiology and it is furthermore frequently accompanied by structural abnormalities of the mitral valve apparatus (Maron et al., 1996). Additionally, myocardial ischemia in the absence of coronary artery disease contributes to the patient's heart failure symptoms and disease progression, as well as general diastolic dysfunction.

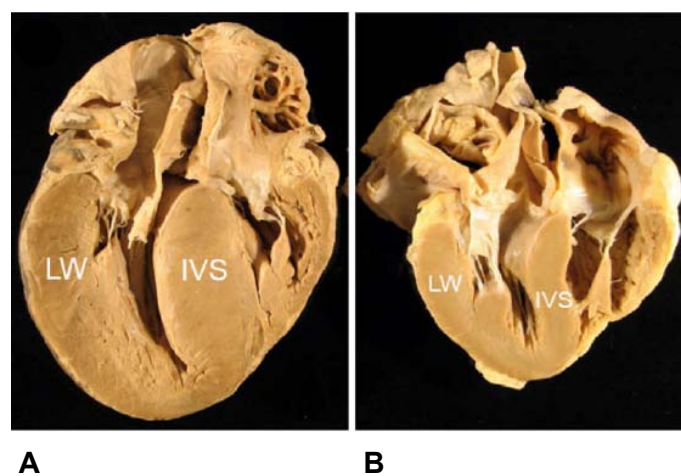


Figure 1.1: (A) A longitudinal section of a patient's heart, exhibiting hypertrophy of the left ventricle's lateral wall (LW) and interventricular septum (IVS). (B) Normal heart (adapted from Ho, 2009)

Histopathologically, hypertrophy of the single myocyte and disorganization in cell arrangement can be detected. Abnormal intramural vessel architecture and interstitial fibrosis occupy large areas of the patient's myocardium (Figure 1.2; Sherrid, 2006).

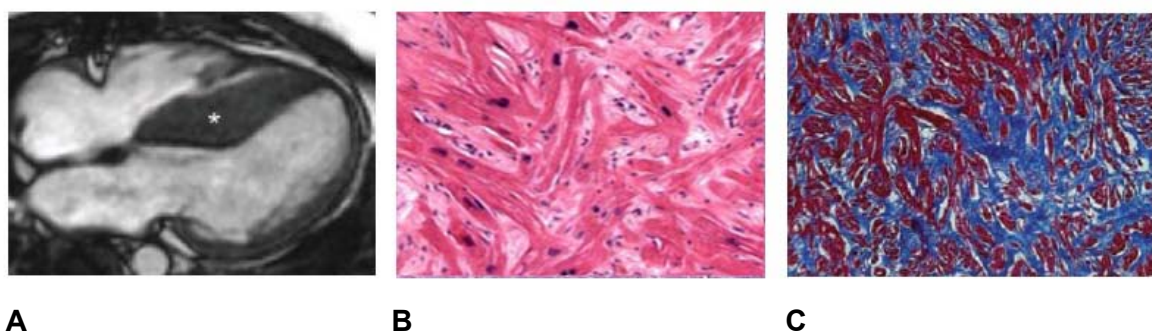


Figure 1.2: Key features of HCM (A) Cardiac magnetic resonance four-chamber view showing asymmetric left ventricular hypertrophy localized at the ventricular septum. (B) Myocardial disarray in surgical myectomy sample. (C) Interstitial fibrosis, collagen stained in blue (adapted from Ho, 2009; Olivotto, 2009).

Due to these findings the frequent observation of electrophysiological transmission impairment and the risk of sudden cardiac death based on arrhythmia seem very comprehensible. The diagnosis of HCM relies on the patient's disposition to symptoms. In some cases the patient is primary diagnosed after sudden cardiac death. Especially during exercise, the disorder's first manifestation can be fatal, making it the most prevalent cause of sudden death in young athletes (Maron et al., 1996).

1.2 Mutations in cardiac myosin-binding protein C gene

Already the first modern description of hypertrophic cardiomyopathy noted its hereditary transmission (Teare, 1958). Today it is well determined that in about 70% of cases a familial background can be detected, following an autosomal-dominant transmission (Maron et al., 1984). If the hereditary relation is determined, HCM is also considered as familial HCM (FHC; for review, see Bonne et al., 1998). Of more than 500 mutations in at least 19 genes, that have been so far identified, most are located in *MYH7* (44%) encoding β -myosin heavy-chain, and in *MYBPC3* (34%) encoding cardiac myosin-binding protein C (cMyBP-C; for review, see Schlossarek et al., 2011).

MyBP-C was first discovered by Offer et al. as a component of striated muscle cells (1973). Today we know three isoforms of MyBP-C: the cardiac, the slow skeletal and the fast skeletal (Winegrad, 1999). To understand the speculated functions of cMyBP-C it is necessary to be aware of the complex structure and function of cardiac muscle tissue.

The heart's muscle tissue consists of cardiomyocytes allowing the cardiac contraction-relaxation cycle. Several cardiomyocytes form a myofiber, which is held together by surrounding collagen connective tissue. At the same time each myocyte is surrounded by a complex cell membrane, the sarcolemma, which also invaginates into the cell's interior, ensuring a connection to the extra cellular space. Bundles of fibrous elements, called myofibrils, fill out the myocyte's cytoplasm. A myofibril is organized into repeated subunits of contractile protein filaments. These subunits are called sarcomeres (Figure 1.3). The sarcomere is the actual contractile unit with the thick myosin filament, the thin actin filament and the interacting proteins. Investigated under the light microscope, the alignment of proteins creates a specific pattern of bands, which is responsible for the histological striated appearance of cardiac and skeletal muscle tissue (Figure 1.3). The sarcomere is defined as the distance between two Z-lines (from the German "Zwischenscheibe"), to which the thin actin filaments are attached. Conversely, the thick myosin filaments extend from the center of the sarcomere (named M-Line) in either

direction towards the Z-lines, though not reaching them. During muscle contraction, the actin filaments move inward towards the center of the sarcomere and draw the Z-lines closer together, shortening the whole sarcomere. A third protein filament, named titin, connects the Z-line to the M-line and hereby stabilizes the thick myosin filament.

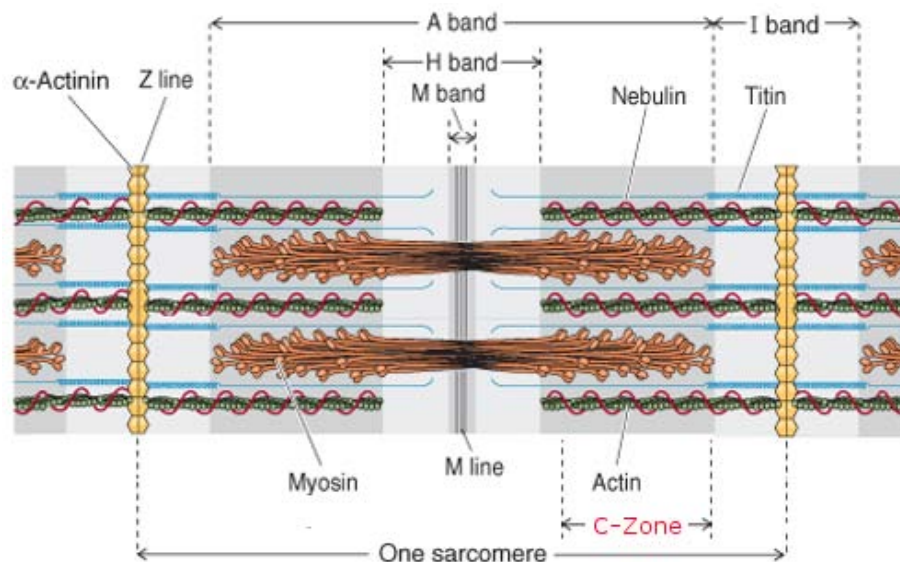


Figure 1.3: Schematic structure of the sarcomere (adapted from Boron and Boulpaep, 2009)

The sarcomere's actual contraction process is ensured by the interaction of myosin and actin supported by a set of 3 proteins called troponins (Figure 1.4), which are well known for their importance in acute coronary syndrome diagnostics (Scirica et al., 2004). Physiologically, troponins represent the acceptor of the actual contraction trigger, which is intracellular calcium increase. The movement of the thick myosin filament against the thin actin filament is an energy consuming process, ensured by adenosine triphosphate (ATP) hydrolysis. A lack of ATP inhibits myosin releasing from the thin filament and is considered as the explanation for rigor mortis (Bear, 2006).

Within this complex structure of the sarcomere cMyBP-C is localized in the cross-bridged bearing zone (C-Zone) of the A-Band (Figure 1.3; Figure 1.4). It is found in regularly spaced intervals and is hypothesized to act as a "barrel hoop", which is stabilizing the thick myosin filaments (for review, see Schlossarek et al., 2011). In addition, a modulating function could be demonstrated: cMyBP-C protein has four known phosphorylation sites, which can be regulated by phosphorylation through different kinases such as cAMP-dependent protein kinase (PKA) and others (Sadayappan et al., 2005; Cuello et al., 2011). As a result of this adrenergic stimulation, cardio protective effects, as well as an increase in force of contraction were demonstrated (Pohlmann et al., 2007).

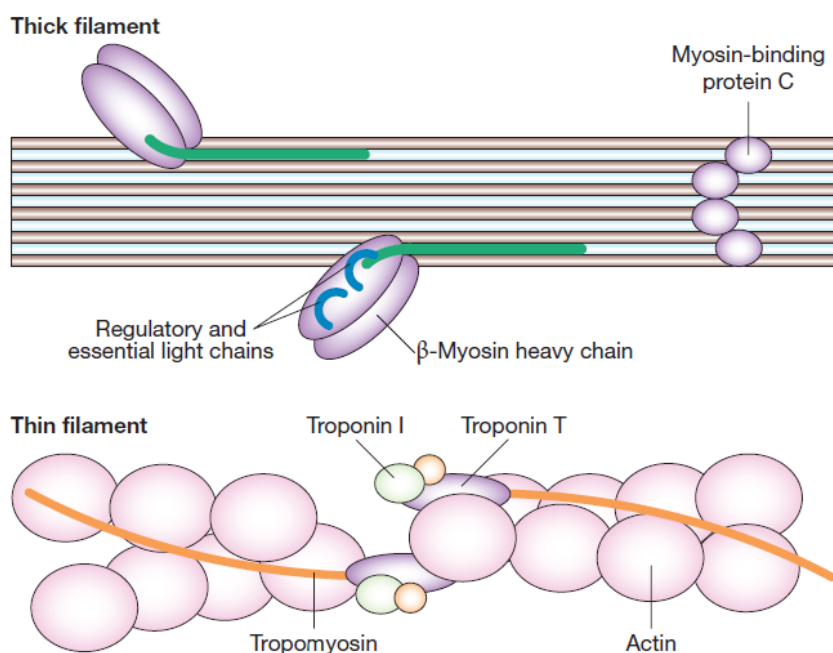


Figure 1.4: Schematic diagram of the cardiac contractile proteins (adapted from Keren, 2008)

Most of the mutations in *MYBPC3* are either frameshift or nonsense mutations, which are supposed to encode truncated protein products (Carrier et al., 1997). Nevertheless truncated proteins, due to a premature stop codon in the mRNA transcript, so far could not be detected in human tissue samples (Rottbauer et al., 1997; Moolman et al., 2000).

Currently there are predominantly two mechanisms discussed, by which these mutations could induce the phenotype of HCM. One explanation might be direct negative effects of the mutant cMyBP-C itself on the sarcomere structure, making the protein a “poison polypeptide” (Carrier et al., 2004). In contrast the reduction of efficient protein, considering the encoding allele a “null allele”, could lead to functional haploinsufficiency and altered sarcomere structures (Seidman et al., 2001). In addition to its direct impact on the sarcomere structure, there are also indications that *aberrant* cMyBP-C interferes with other cell functions such as protein degradation (for review, see Schlossarek et al., 2011). Hereby mutant cMyBP-C might contribute indirectly to the pathogenesis of HCM.

1.3 Disturbances of protein degradation in hypertrophic cardiomyopathy

It was demonstrated that truncated mutant cMyBP-C impairs the proteolytic capacity of the ubiquitin-proteasome system in neonatal rat cardiomyocytes (Sarikas et al., 2005). The ubiquitin-proteasome system degrades the majority of cellular proteins and is essential for a physiological equilibrium between protein synthesis and degradation in all eukaryotic cells (for review, see Dahlmann, 2007). It consists of different subunits, which

are either involved in substrate recruitment by ubiquitination or substrate degradation by proteolysis. Substrate recruitment for the proteasome is ensured by three enzymes (Ligases E1-3) which are responsible for the ATP-dependent ubiquitin activation and afterwards its ligation to the target protein (for review, see Mearini et al., 2008). Repeated cycles of this process result in a polyubiquitylated substrate protein that is recognized by the proteolytic machinery of the system. Although there are in principal three different beta-subunits sharing the same proteolytic mechanism, different substrate specificities can be detected due to interactions with local residues near the active sites of each subunit (Harris et al., 2001). The chymotrypsin-like, the trypsin-like and the caspase-like activities are the actual proteolytic mechanisms and can be measured using fluorogenic substrates (see 2.2.3.4). The mechanisms by which the ubiquitin-proteasome system can disturb cell integrity are manifold. Genetic defects in any involved enzyme, as well as generally altered levels of activity can have adverse effects on many diseases (for review, see Dahlmann, 2007).

Another system of protein quality control is the nonsense-mediated mRNA decay (NMD). The NMD is a cellular surveillance mechanism preventing the translation of nonsense mRNA (for review, see Maquat, 2005). A recent study demonstrated the involvement of both the UPS and NMD in the degradation of mutant cMyBP-C proteins and mRNA, respectively in *Mybpc3*-knock-in (KI) mice (Vignier et al., 2009). High activity levels of both of these systems in 9-week-old KI mice illustrate the complex regulation of the expression of *Mybpc3* mutations and suggest relevance to pathology in case of their failure (Vignier et al., 2009). Thus, there is increasing evidence of involvement of quality control systems in the pathogenesis of HCM. Supporting this hypothesis recent studies were able to demonstrate reduced proteasome activity in human tissue samples of HCM patients (Predmore et al., 2010), as well as accumulation of ubiquitinated proteins in KI mice (Vignier et al., 2009). Considering these results, cellular responses to counteract the demonstrated disturbances of protein homeostasis in HCM seem indispensable.

1.4 Endoplasmic reticulum stress and the unfolded protein response

The endoplasmic reticulum (ER) plays an important role in cellular homeostasis. It is a rich Ca^{2+} -storage and mediates synthesis, folding and maturation of cellular and secretory proteins. Due to its function in protein synthesis and folding, calcium homeostasis and lipid biosynthesis, the ER lumen contains a specialized environment for proper protein assembly (Kitakaze et al., 2010). Disruptions to this environment, potentially resulting in unfolded or misfolded proteins, are considered as ER stress. Additionally ER overload,

oxidative stress, hypoxia and disturbances of calcium homeostasis have been demonstrated to disturb the ER integrity and cause stress (for review, see Minamino et al., 2010). In 1988 the investigation of calcium homeostasis within the ER revealed responses to ER stress. Since then, these responses are known as a set of three transcriptional and translational pathways entitled as the unfolded protein response (UPR; Kozutsumi et al., 1988; Figure 1.5).

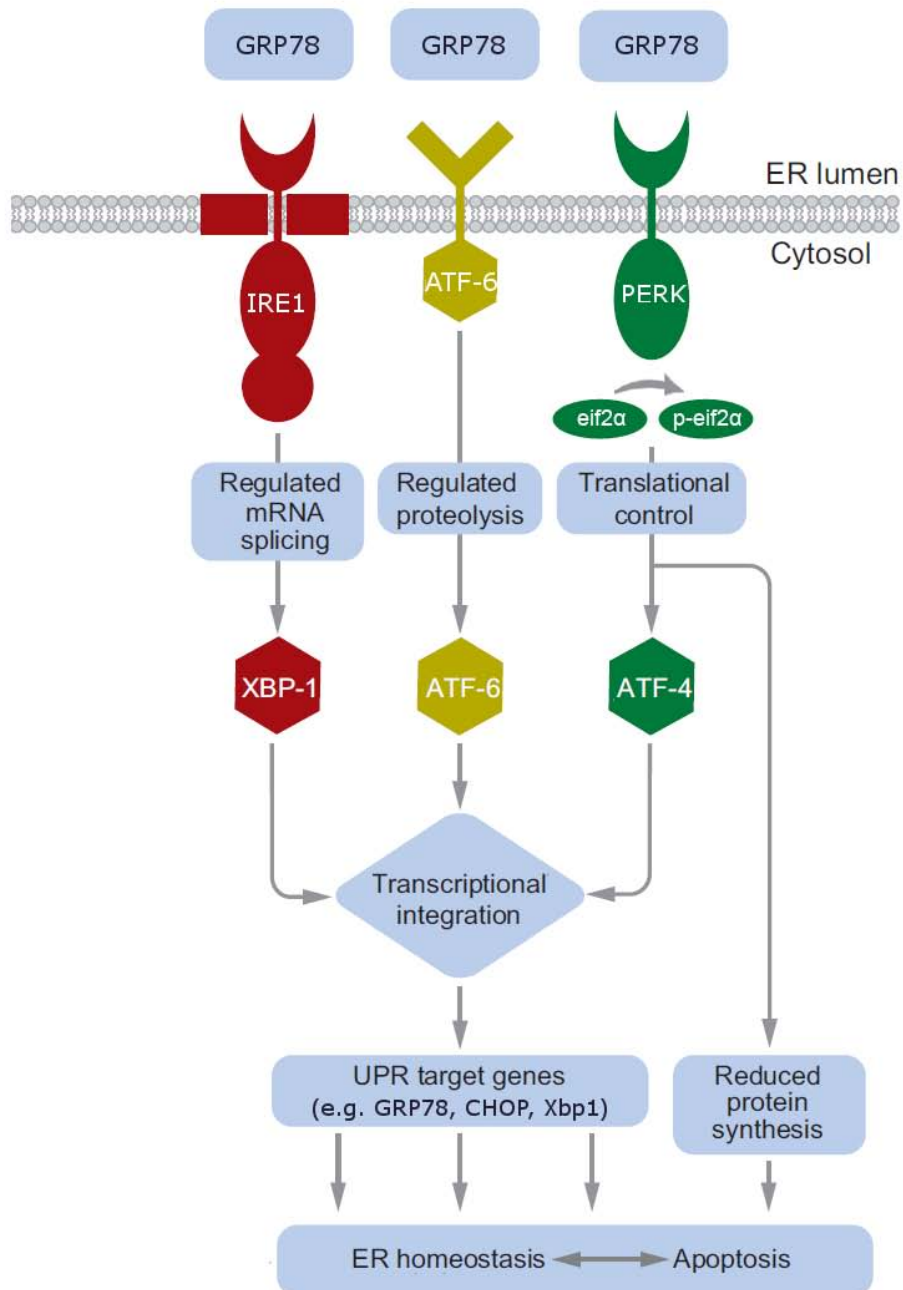


Figure 1.5: A schematic of the unfolded protein response (adapted from Lin, 2008)

Generally, the UPR's response to disturbances can be either adaptive by trying to restore misfolded proteins and attenuate synthesis, or in case of failure, proapoptotic. Each pathway is mediated by a different receptor protein localized in the ER membrane: PK-like ER kinase (PERK), activating transcription factor 6 (ATF6), and inositol-requiring enzyme 1 (IRE1). These UPR sensors have their N-termini in the lumen of the ER and their C-termini in the cytosol, thereby connecting the ER and the cytosol (for review, see Ron et al., 2007). Their activation relies on different factors which are still subject of investigation. Yet it was shown that the most decisive factor is the interaction of the sensors with the glucose-regulated protein 78 (GRP78), a prominent ER heat shock protein, also known as a molecular chaperone (Bertolotti et al., 2000). Inactivated, each receptor binds GRP78, while accumulation of immature or misfolded proteins leads to the dissociation of GRP78 from the receptor and therefore to the activation of the pathways. Hereby the level of activation is directly determined by the level of accumulating protein.

The first branch of the three pathways is initiated by IRE1, the most fundamental ER stress sensor, which was shown to be conserved across many organisms from yeast to humans (Tirasophon et al., 1998). Its activation is followed by dimerization and autophosphorylation, enabling an endoribonuclease activity. This unconventional mechanism is required to specifically cleave the mRNA encoding the messenger molecule X-box binding protein 1 (XBP-1). Only the cleaved XBP-1 mRNA can be translated to the transcriptionally active XBP-1 protein, which is able to bind and regulate the promoters of many UPR target genes within the nucleus (Tirasophon et al., 1998).

The second pathway is initiated by ATF6. This second ER stress sensor, a basic zip family transcription factor, is as well regulated by the concentration of GRP78 (Ron et al., 2007). Its dissociation from the receptor is followed by the translocation of ATF6 to the Golgi apparatus, where it is cleaved into its active cytosolic fragment, now capable to bind to many promoters of UPR target genes within the nucleus. Of those most important is the CCAAT/enhancer-binding protein homologous protein, better known as CHOP, a potent pro-apoptotic factor (Ma et al., 2003). The exact mechanism by which CHOP induces cell death is still not completely understood. Yet, it was shown that it interferes in the balance in the amounts of B-cell lymphoma (Bcl)-2 family proteins, which have been implicated in a large number of cancers and therefore emphasizes its function in cell cycle control (Galehdar et al., 2010). Interestingly, in addition to its pro-apoptotic function ATF6 establishes a feedback loop by co-regulating the transcription of XBP-1 (Toko et al., 2010).

The third UPR pathway is initiated by PERK, which carries a serine threonine kinase that phosphorylates eukaryotic translation initiation factor 2 α (eIF2 α). Unphosphorylated, eIF2 α mediates the assembly of the ribosome complex, thus initiating translation, while this function is abolished by phosphorylation (Ron et al., 2007). Hereby protein accumulation is encountered by protein synthesis attenuation. Paradoxically, it was shown, that some proteins require the phosphorylation of eIF2 α for their translation, as it is the case with activating transcription factor 4 (ATF4), which targets few genes necessary to maintain the UPR (Minamino et al., 2010). In this way the third UPR pathway ensures general attenuation of translation, accompanied by the selective increase of proteins necessary to antagonize cell disturbances. Additionally, just like the second branch of the UPR, ATF4 is capable to increase the transcription of CHOP (Ma et al., 2003).

Cooperating, the three arms of the UPR regulate various genes encoding ER chaperones, antioxidants, apoptotic factors and many others. Upon activation, concentration of GRP78, CHOP and others is increased to counteract the metabolic disturbance. However, in addition to protein synthesis regulation and potential apoptotic signaling, the ER is also involved in general protein degradation through the ER-associated protein degradation (ERAD) pathway. Through this mechanism, the ER mediates migration of misfolded proteins to the cytosol, linking them to the ubiquitin-proteasome system (Tsukamoto et al., 2010).

Considering the functional complexity of the UPR, ranging from cell disturbance adaptation to apoptosis, it seems obvious that failure of the UPR holds capacious pathologic potential. Already, there are some concrete and well understood examples of both UPR insufficiency and UPR abundance leading to pathogenic conditions.

1.5 The unfolded protein response as cause of disease

Studies on Alzheimer's disease revealed interactions of mutated proteins and IRE1 following a poison polypeptide mechanism (Katayama et al., 1999). In this investigation, it was detected that Presenelin-1 (PS1), which is the most frequently mutated gene in cases of familial Alzheimer's disease, binds to IRE1 and blocks further downstream signaling within the pathway in cultures of neuroblastoma cells. The hereby suspected impairment of the UPR was supported by decreased levels of GRP78 and increased vulnerability of cells to ER stress conditions. Interestingly, the researchers were able to almost completely restore the resistance to ER stress in virus infected cells overexpressing

GRP78. Possible targets of treatment research suggest themselves.

Studies on diabetes mellitus identified frameshift mutations in the human *EIF2AK3* gene encoding PERK, which cause hereditary diabetes, known as the Wollcott-Rallison syndrome (Delepine et al., 2000). In this case, it is presumed that due to the mutation failure of the UPR itself to handle increasing concentrations of misfolded insulin causes death of the pancreatic beta cells. These findings were supported by observations in a PERK (-/-) knock-out mouse model developing early onset diabetes (Harding et al., 2001).

Another example in the field of degenerative diseases gives evidence to cases of UPR *high activity malfunctioning* due to a protein overload of the ER: There are implications that increased UPR activity contributes to the pathogenesis of retinitis pigmentosa (RP), which is the most common cause of inherited blindness through the loss of photoreceptor neurons (Shintani et al., 2009). Earlier studies already had shown that mutations in the gene encoding P23H-rhodopsin, the most frequent mutation causing RP in the USA, will cause aggregates of misfolded rhodopsin within the ER (Kaushal et al., 1994). While it had remained ambiguous in which way this affects the extensive photoreceptor extinction for a long time, finally a study was able to show that P23H-rhodopsin expression in *Drosophila* triggered a robust UPR activation, which implicates that neuron extinction is caused by UPR triggered apoptosis (Ryoo et al., 2007).

In summary, the mentioned examples illustrate well the diversity of UPR conditions. In some states of disease it might be beneficial to suppress certain outputs of the UPR, whereas in others an induction may provide enhancing effects. In contrast to these concrete examples of pathogen involvement of the UPR, comparably little is known about the impact of the UPR on cardiovascular disease. Besides, one has to keep in mind, that the endoplasmic reticulum is a cell organelle, capable of distinct specificity in different tissues (Kitakaze et al., 2010). Considering the cardiomyocyte's *sarcoplasmic reticulum*, investigations were capable to demonstrate UPR activation in both hypertrophic and failing hearts (for review, see Minamino et al., 2010). Interestingly, in this case failing hearts exhibited higher concentrations of CHOP, suggesting UPR-dependent apoptosis as a cause of increasing insufficiency.

1.6 Aim of the thesis

While there is increasing evidence of involvement of the UPR in the spectrum of neuronal and diabetic disorders, comparatively little is known about its involvement in cardiac disease. However the mechanisms of a pathologic UPR in different diseases might be similar in others, such as HCM. By assuming that the effects of mutant cMyBP-C contribute strongly to HCM's pathogenesis, it is quite obvious to expect an involvement of the UPR in HCM due to protein homeostasis disturbances.

To gain insights into this topic, we used two mouse models. The first HCM mouse model carries a *Mybpc3*-knock-in mutation (KI) causing LVH with reduced fractional shortening. Only a low level of mutant cMyBP-C (10% of normal) was detected in this model due to a regulation by both the NMD and the ubiquitin-proteasome system (Vignier et al., 2009). On the other hand, the second model of homozygous *Mybpc3*-deficient mice (KO) also exhibits LVH with reduced fractional shortening, but does not express any *Mybpc3*, thus serving as a pure model of cMyBP-C insufficiency (for review, see Schlossarek et al., 2011). Furthermore both models were crossed with Ub^{G76V}-GFP transgenic mice, which monitor the global activity of the ubiquitin-proteasome system (Lindsten et al., 2003).

In the first part of this project, we evaluated whether constant degradation of mutant cMyBP-C induces saturation of the ubiquitin-proteasome system and therefore accumulation of (ubiquitinated) proteins with age in KI, but not in KO mice

In the second part of this project, we evaluated whether the UPR is activated in response to impairment of the ubiquitin-proteasome system. We focused on a detailed analysis of the particular components of the UPR in KI mice, using the KO model as control.

In the last part of this study, we induced ER stress in KI-neonatal mouse cardiomyocytes (KI-NMCM) with two drugs, known to induce the UPR. The first one, tunicamycin, is an inhibitor of N-glycosylation and hereby blocks glycoprotein synthesis (Iwata et al., 2005). The second, thapsigargin, raises cytosolic Ca²⁺ concentration by blocking the endoplasmic reticulum Ca²⁺ ATPase (SERCA; Rogers et al., 1995). Both drugs reliably increase cellular ER stress and are used routinely for UPR induction.

2 Material and Methods

2.1 Material

2.1.1 Animals

The investigations conform to the guide for the care and use of laboratory animals published by the NIH (Publication No. 85-23, revised 1985).

2.1.1.1 The *Mybpc3*-knock-out mouse model

The KO mouse model was created by Lucie Carrier in Paris on a blackswiss background (Carrier et al., 2004). Exons 1 and 2 of the mouse *Mybpc3* gene, including the transcription initiation site were deleted by homologous recombination. cMyBP-C mRNA and protein cannot be detected in KO mice, validating gene inactivation. Development of LVH with decreased fractional shortening, as well as a significant increase of LV mass to body weight ratio at the age of 3-4 months compared to wild type littermates, could be determined by echocardiography. Histologically, interstitial fibrosis, calcification of fibrotic areas and myocardial disarray could be examined at this age.

2.1.1.2 The *Mybpc3*-knock-in mouse model

The KI mouse model was developed in Paris by Nicolas Vignier and Lucie Carrier. The G>A transition on the last nucleotide of exon 6 was introduced in mice by gene targeting using the Cre/lox system as depicted in Figure 2.1.

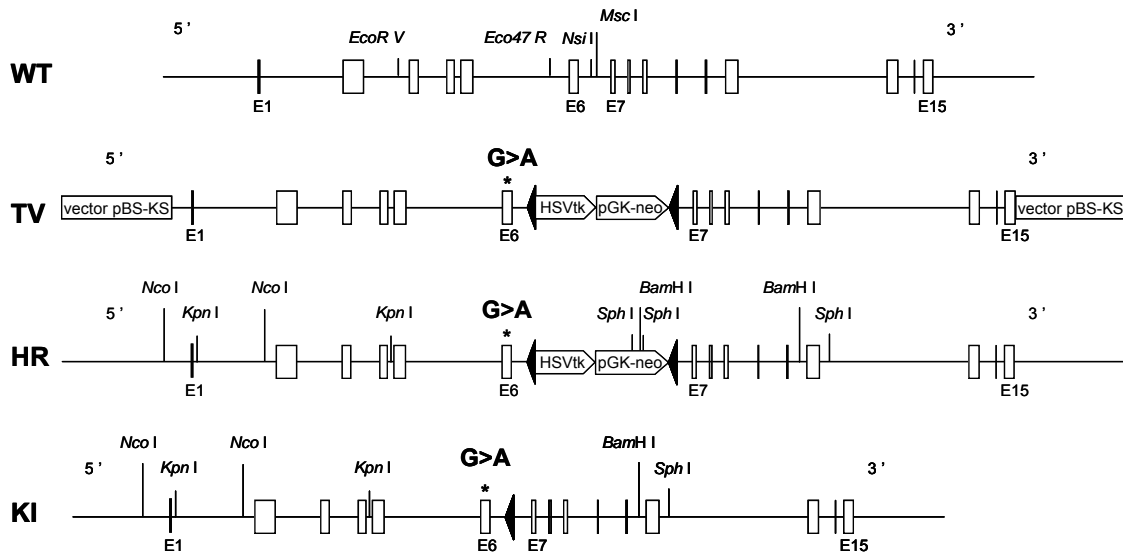


Figure 2.1: Targeting strategy for the *Mybpc3* knock-in mouse model. WT, schematic structure of the mouse *MYBPC3* gene from exon 1 (E1) to exon 15 (E15); TV, targeting vector containing the *G>A* transition on the last nucleotide of exon 6 (E6) and the selection cassette (herpes simplex virus thymidine kinase (HSVtk), pGK-neomycin (pGK-neo)) flanked by two *loxP* sites (black arrows); HR, allele obtained after homologous recombination in AT1 embryonic stem cells; KI, targeted floxed-out knock-in allele.

The targeting vector containing a 12.5-kb insert was obtained in several steps. A 8105-bp fragment containing the 5'-part of the mouse *MYBPC3* gene, which covers 1747-bp upstream of exon 1 up to exon 15, was obtained by long-range polymerase chain reaction (PCR) and cloning from a FIX II genomic library derived from a 129/Svj mouse strain, and then cloned into the pBluescript® II KS+ vector. The *G>A* transition on the last nucleotide of exon 6 was obtained by site-directed mutagenesis on a 258-bp PCR fragment, which was then cloned into the *Eco47RI*-*NsiI* sites. The linearized targeting vector, which contained the mutation and a selection cassette composed of the neomycin resistance and herpes simplex virus thymidine kinase genes flanked by two *loxP* sites, was electroporated into AT1 embryonic stem cells and proceeded for homologous recombination (Buchou et al., 2003). Genomic DNA was extracted from G418 resistant clones and screened by long-range PCR to check for 5' and 3' homologous recombination. Two clones with the correct recombination event were used to obtain germ-line transmitting chimeras (Buchou et al., 2003). One chimeric mouse was obtained and crossed with a Black-swiss wild-type mouse to check for germline transmission. Two heterozygous *Mybpc3* knock-in females were crossed with a CD1 Sycp1-Cre transgenic male, which expressed the recombinase Cre under the control of the Sycp-1 promoter (Vidal et al., 1998). After Cre-mediated recombination, one *loxP* site remained in the DNA, which resulted in a 94-bp longer PCR fragment. Heterozygous offsprings were further backcrossed to Black-swiss mice. Pups were born in the expected Mendelian ratios of wild-type, heterozygous and homozygous *Mybpc3* knock-in mice. Both heterozygous and homozygous *Mybpc3* knock-in mice appeared normal and were viable up to two years.

2.1.1.3 The Ub^{G76V}-GFP mouse model

The Ub^{G76V}-GFP mouse model was kindly given by Nico Dantuma (Microbiology and Tumor Biology Center, Karolinska Institute, Stockholm). This mouse model expresses an Ub^{G76V}-GFP reporter protein, which is a N-terminal mutant ubiquitin (Ub^{G76V}) in frame with a green fluorescent protein (GFP) under the control of a chimeric cytomegalovirus immediate early (CMV-IE) enhancer and a chicken β -actin promoter (Lindsten et al., 2003; Figure 2.2).

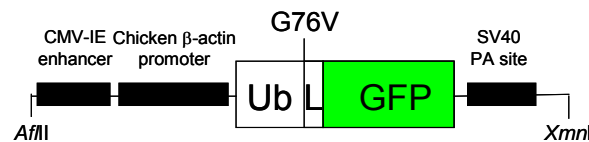


Figure 2.2: Schematic illustration of the transgenic construct of the Ub^{G76V}-GFP mice. The transgene contains the CMV-IE enhancer, the chicken β -actin promoter, the Ub^{G76V}-GFP open reading frame and the SV40 polyadenylation signal. Restriction sites used for transgene excision are indicated (adapted from Lindsten et al., 2003).

Ub^{G76V}-GFP transcripts were present in different tissues, with predominant expression in skeletal muscle, heart, testis and cerebellum. The N-terminal-linked ubiquitin molecule serves as an acceptor for polyubiquitin chains through the canonical Lys48 and the less common Lys29 (Lindsten et al., 2003). The G76V substitution prevents the removal of this ubiquitin by cellular ubiquitin C-terminal hydrolases, leading to efficient ubiquitination and proteasomal degradation of the Ub^{G76V}-GFP fusion protein. Therefore, no GFP-fluorescence in any of the tissues was obtained in cryosections from adult Ub^{G76V}-GFP mice by fluorescence microscopy under normal conditions. In contrast, after treatment with different proteasome inhibitors, pronounced accumulation of the Ub^{G76V}-GFP reporter was visualized in primary fibroblasts and neonatal cardiomyocytes (Lindsten et al., 2003). The intraperitoneal (i.p.) injection of the proteasome inhibitor MG262 (5 μ mol/kg) in adult Ub^{G76V}-GFP mice resulted in a detectable GFP fluorescence in the liver, small intestine, pancreas, kidney and to a lower extent in the lung and spleen. No fluorescent cells could be observed in the brain, heart and skeletal muscles (Lindsten et al., 2003).

2.1.2 Chemicals

Acrylamide/bis solution (29:1)	Bio-Rad®
Adenosine 5'-triphosphate (ATP)	Sigma
Ammonium persulfate (APS)	Bio-Rad®
AmpliTaq Gold® polymerase	Applied Biosystems

Aqua ad injectabilia	Baxter GmbH [®]
Bovine serum albumin (BSA)	Sigma [®]
Bromophenol blue	Merck [®]
Complete mini-proteases inhibitor cocktail	Roche Diagnostics [®]
Coomassie Brilliant Blue G-250 reagent	Bio-Rad [®]
Deoxyribonucleotide triphosphate (dNTP) mix	Applied Biosystems
Dimethyl sulfoxide (DMSO)	Sigma [®]
Dithiothreitol (DTT)	Sigma [®]
Dulbecco's modified Eagle medium (DMEM) with 4.5 g/L glucose and without pyruvate	Gibco [®]
ECL plus Western blotting detection system	Amersham Biosciences
Ethidium bromide	Fluka [®]
Ethylenediaminetetraacetic acid (EDTA)	Sigma [®]
Fetal bovine or calf serum (FBS or FCS)	Biochrom [®]
Glycerol	Merck [®]
Horse serum	Biochrom [®]
Hydrochloric acid (HCl)	Merck [®]
4-(2-hydroxyethyl)piperazine-1-ethanesulfonic acid (HEPES)	Roth
Immunoglobulin G	Sigma [®]
Isotonic 0.9% sodium chloride solution	Baxter GmbH [®]
Loading dye, 6x	Fermentas [®]
M199 with Earl's salt and L-glutamine	Gibco [®]
Magnesium acetate tetrahydrate (Mg(CH ₃ COO) ₂ ·4H ₂ O)	Merck [®]
Magnesium chloride hexahydrate (MgCl ₂ ·6H ₂ O)	Roth [®]
Maxima [™] Probe/Rox qPCR Master Mix	Fermentas [®]
Maxima [™] SYBR Green/Rox qPCR Master Mix	Fermentas [®]
Methanol	J. T. Baker [®]
Milk powder	Roth [®]
Penicillin-streptomycin	Gibco [®]

Phosphate buffered saline (PBS)	Biochrom®
Phosphocreatine	Calbiochem®
Phosphocreatinekinase	Sigma®
Ponceau S	Serva®
Potassium chloride (KCl)	Merck®
Precision Plus Protein Standard™	Bio-Rad®
Sodium chloride (NaCl)	J. T. Baker®
Sodium dodecyl sulfate (SDS)	Roth®
Sodium fluoride (NaF)	Merck®
Sodium hydrogen carbonate (NaHCO ₃)	Merck®
Sodium hydroxide (NaOH)	Merck®
Succinyl-leucyl-leucyl-valyl-tyrosyl-7-amino-methylcoumarin (SUC-Leu-Leu-Val-Tyr-AMC)	Calbiochem®
SuperSignal® West Dura extended duration substrate	Pierce®
TaqMan® Universal PCR Master Mix	Applied Biosystems
Tetramethylethylenediamine (TEMED)	Bio-Rad®
Thapsigargin	Sigma Aldrich®
Trishydroxymethylaminomethane (Tris) base	Sigma®
Tris hydrochloride (Tris-HCl)	Promega®
Tunicamycin	Sigma Aldrich®
Polyoxyethylene (20) sorbitan monolaurate (Tween® 20)	Sigma®

2.1.3 Chemicals with risk (R-) and safety (S-) phrases

Acrylamide/bis solution	R: 23/24/25-45-46-48	S: 36/37/39-45-60
ATP	R: -	S:22-24/25
APS	R: 8-22-36/37/38-42/43	S: 22-24-26-37
Bromphenol blue	R: -	S:22-24/25

Coomassie Brilliant BlueG-250 reagent	R: 20/21/22-34-68	S: 26-36/37/39-45
DMSO	R: 36/37/38	S: 23-26-36
DTT	R: 22-36/37/38	S: 26-36
ECL plus Western blotting detection system	R: 11-19-36/37-40-66	S: 16-23-36/37
Ethidium bromide	R: 23-68	S: 36/37-45
EDTA	R: 36-52/53	S: 26-61
Glycine	R: -	S: 22-24/25
Hydrochloric acid	R: 34-37	S: 26-36/37/39-45
Magnesium acetate tetrahydrate	R: -	S: 22-24/25
Methanol	R: 11-23/24/25-39	S: 7-16-36/37-45
PBS	R: -	S: 22-24/25
Ponceau S	R: 36/37/38-51/53	S: 2-25-26-29/56-37-46-57-60-64
Potassium chloride	R: -	S: 22-24/25
SDS	R: 22-36/38	S: 22-24/25
Sodium fluoride	R: 25-32-36/38	S: 22-36-45
Sodium hydroxide	R: 35	S: 26-37/39-45
TEMED	R: 11-20/22-34	S: 16-26-36/37/39-45-60
Tris base	R: 36/37/38	S: 26-36
Tris hydrochloride	R: 36/37/38	S: 26-36

2.1.4 Antibodies

Anti-calsequestrin, polyclonal	Dianova [®]
Anti-GFP (FL), polyclonal	Santa Cruz Biotechnology [®]
Anti-GRP78, polyclonal	Stressgen [®]

Anti-IRE1 α , polyclonal	Cell Signaling [®]
Anti-p-eIF2 α , polyclonal	Cell Signaling [®]
Anti-rabbit IgG peroxidase conjugate	Sigma and Dianova [®]
Anti-mouse IgG peroxidase conjugate	Dianova [®]

2.1.5 Kits

RevertAid [™] First Strand cDNA Synthesis Kit	Fermentas [®]
SV Total RNA Isolation Kit	Promega [®]

2.1.6 Oligonucleotides

All primers and probes were designed using the Primer Express software or the Primer3 program, which is online available, and purchased from the MWG Biotech AG.

2.1.7 Consumable Materials

Blotting paper (Whatman 3MM)	Schleicher & Schuell [®]
Cell scraper	Sarstedt AG & Co.
Cell strainer	Becton Dickinson
Culture plates (12-well)	Nalge Nunc International
Cuvettes (10 x 4 x 45 mm)	Sarstedt AG & Co. [®]
Falcon tubes (15 and 50 ml)	Sarstedt AG & Co. [®]
Latex gloves	Paul Hartmann AG [®]
Micro tubes (1.5, 2.0 ml)	Sarstedt AG & Co. [®]
Multiple well plate (384-wells)	Sarstedt AG & Co. [®]
Nitrile gloves	Ansell [®]

Nitrocellulose membrane (Protran [®] BA 85)	Schleicher & Schuell [®]
Nylon membrane (Hybond N+)	Amersham Biosciences [®]
PCR Tubes	Sarstedt AG & Co. [®]
Pipette tips (for 10, 100 and 1000 µl pipettes)	Sarstedt AG & Co. [®]
Serological pipettes (2, 5, 10 and 25 ml)	Sarstedt AG & Co. [®]
Serological pipettes (10 ml, wide tip)	Becton Dickinson [®]
Sterile filter (0.22 µm)	Sarstedt AG & Co. [®]

2.1.8 Laboratory Equipment

Accu-jet pipetting aid	Brand GmbH [®]
Analytical balance (GENIUS)	Sartorius AG [®]
Benchtop centrifuge	Sarstedt AG & Co. [®]
Blotting system (Mini Trans-Blot [®] cell)	Bio-Rad [®]
Centrifuge (5810 R)	Eppendorf AG [®]
Chemie Genius ² Bio imaging system with Gene Tools software	Syngene [®]
Electrophoresis system (Mini PROTEAN [®] 3 electrophoresis cell)	Bio-Rad [®]
Ice machine	Scotsman [®]
Incubators (B 5050 E and Hera cell 240)	Heraeus Instruments
Magnetic stirrer (IKAMAG [®] RCT)	Janke & Kunkel GmbH [®]
Microplate reader (Tecan Safire ²)	Tecan [®]
Microcentrifuge (5415 R)	Eppendorf AG [®]
Microwave	Sharp [®]
Neubauer chamber	Glaswarenfabrik Karl Hecht KG [®]
PCR cycler (GeneAmp [®] PCR system 9700)	Applied Biosystems

pH-meter	Knick GmbH®
Pipettes (10, 100, 1000 µl)	Eppendorf AG®
Portable balance (Scout™ Pro)	Ohaus®
Power supply	Bio-Rad®
Precision balance (Precision Advanced)	Ohaus®
Spectrophotometer (Smart Spec™ 3000)	Bio-Rad®
Surgical instruments	Karl Hammacher GmbH®
Sterile work bench (Lamin Air HB 2448)	Heraeus Instruments®
Taqman ABI Prism 7900HT sequence detection system with ABI 7900HT SDS 2.4 software	Applied Biosystems®
Tissue Lyser	Qiagen®
Thermomixer comfort	Eppendorf AG®
Ultra-pure water system Milli-Q plus	Millipore®
Vortexer (Vibrofix VF1)	Janke & Kunkel GmbH®
Water bath	GFL®

2.2 Methods

2.2.1 Organ extraction

Organ extraction was authorized by the Behörde für Soziales, Familie, Gesundheit und Verbraucherschutz der Freien und Hansestadt Hamburg (Org 370). Mice were sacrificed by cervical dislocation in light CO₂ anesthesia and weighted. After median thoracotomy, the hearts were extracted, rinsed in isotonic 0.9% NaCl solution, dried and weighted. After removing the atria, the ventricular weights were determined. Then, tissues were frozen in liquid nitrogen and stored at -80 °C until utilization. To equally portion the ventricles for different preparations, frozen ventricles were powdered with a steel mortar in liquid nitrogen. The tissue powder was mainly divided in three portions and also stored at -80 °C until utilization.

2.2.2 RNA analysis

2.2.2.1 RNA isolation

Total RNA was extracted from ~ 30 mg frozen tissue powder or 3.3×10^5 cultured and treated isolated neonatal mouse cardiomyocytes according to the instruction manual of the SV Total RNA Isolation Kit. Total RNA was stored at -80 °C until further utilization.

2.2.2.2 RNA concentration determination

RNA concentration was determined with a spectrophotometer by measuring the absorbance at a wavelength of 260 nm and assuming that 1 unit of absorbance corresponds to 40 µg/ml of RNA. Absorbance was also determined at the wavelength of 280 nm, and the ratio A_{260}/A_{280} was calculated to test for protein contamination.

2.2.2.3 Reverse transcription (RT)

Total RNA was reverse transcribed into cDNA using oligo(dT)s according to the instruction manual of the RevertAid™ First Strand cDNA Synthesis Kit for RT-qPCR.

2.2.2.4 Quantitative PCR

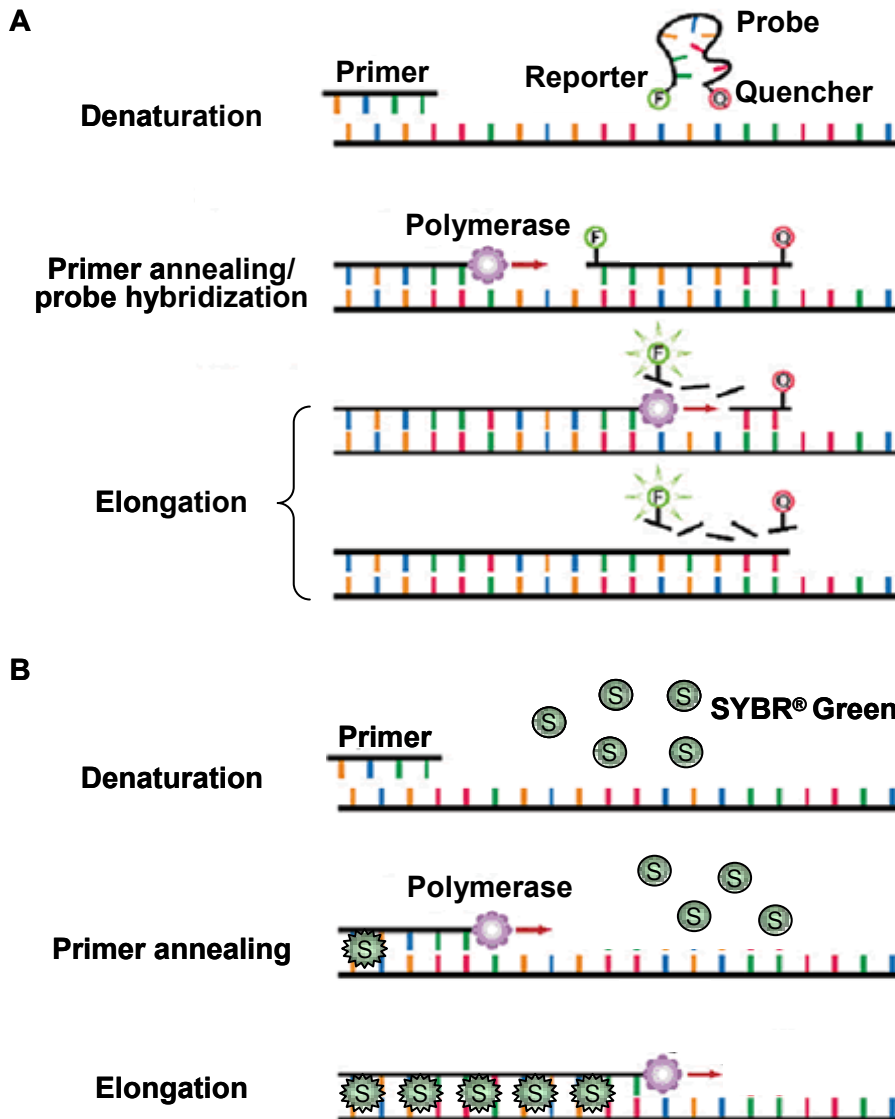


Figure 2.3: Quantitative PCR using A TaqMan[®] probe B SYBR[®] Green (adapted from the Takara Bio USA website)

The quantitative PCRs were performed on the TaqMan[®] ABI Prism[®] 7900HT sequence detection system using specific TaqMan[®] probes or SYBR[®] Green (Figure 2.3). The TaqMan[®] probe is designed to anneal to a specific sequence of the template between the forward and reverse primers. The probe has a high-energy dye termed reporter at its 5'-end and a low-energy molecule termed quencher at its 3'-end. When the probe is intact and excited by a light source, the reporter's emission is suppressed by the quencher as a result of the close proximity of the dyes. Cleavage of the probe by the 5'-exonuclease activity of the polymerase increases the distance between the reporter and quencher and hereby stops the energy transfer. The fluorescent emission of the reporter increases and is directly proportional to the amplification factor. SYBR[®] Green is a dye that unspecifically intercalates

in double-stranded DNA. This intercalation induces a fluorescent emission. After the PCR reaction, a melting curve analysis is required to differentiate between mismatched PCR products (e.g. primer dimers) and perfectly matched fragments.

For all RT-qPCRs, guanine nucleotide binding protein, alpha stimulating (G α S) was used as an endogenous control to balance differences in the amount of cDNA added to each reaction (primers and probes see Table 2.1). To validate the results, single results were compared to normalization to glyceraldehyde-3-phosphate dehydrogenase (GAPDH).

Table 2.1: Primer and probes used for real-time PCR

Primer/Probe name	Primer/Probe Sequence (5'-3')
ATF4 F	CGTGGGTCTCCTCGGCCCAA
ATF4 R	ACACTCGCCAGTGAGGGCCT
Bcl-2 F	CTGCAAATGCTGGACTGAAA
Bcl-2 R	TCAGGAGGGTTTCCAGATTG
Calnexin F	GCAGAGAAGCCAGAGGATTG
Calnexin R	AGGCTTCCATTTGCCCTTAT
Calreticulin F	CAGATTCCAAGCTGAGGAC
Calreticulin R	TCAATTTGACGTGGTTTCCA
CHOP F	CCTAGCTTGGCTGACAGAGG
CHOP R	GGGCACTGACCACTCTGTTT
GAPDH F	TCATTTTGGGGTTTGTTCCT
GAPDH R	GGTTTCCCATCCCCACATAC
GRP78 F	TGCAGCAGGACATCAAGTTC
GRP78 R	TACGCCTCAGCAGTCTCCTT
GRP94 F	AGGGGAGGTCACCTTCAAGT
GRP94 R	TTGGGCATCATATCATGGAA
G α S F	CAAGGCTCTGTGGGAGGAT
G α S R	CGAAGCAGGTCTGGTCACT
G α S probe	AGGAAGTACTGGGCACAGTCGATCAGC
Metallothionein1 F	GGACCCCAACTGCTCCTG
Metallothionein1 R	AGGAGCAGCAGCTCTTCTTG
Ub ^{G76V} -GFP F	GCTCAAGCTTCGAATTCACC
Ub ^{G76V} -GFP R	TCCAGCAAAGATCAGCCTCT
XBP-1 F	GATCCTGACGAGGTTCCAGA
XBP-1 R	GGCAACAGTGTCAGAGTCCA

(Abbreviations: F=forward; R=reverse)

The cDNAs were diluted 1:10 and amplified using the specific primer pair and either the corresponding probe and Maxima™ Probe/Rox qPCR Master Mix or the Maxima™ SYBR GREEN® qPCR Master Mix. The used PCR program is specified in Table 2.2. In cases of analysis using specific probes stage 3 was disregarded.

Table 2.2: PCR program for quantitative RT-PCR

Stage	Temperature (°C)	Time (min:sec)	cycles
Stage 1	95	10:00	1
Stage 2	{ 95 60 }	{ 00:15 01:00 }	45
Stage 3	{ 95 60 95 }	{ 00:15 00:15 00:15 }	1

All analyses were performed in triplicates with the software ABI 7900HT SDS 2.4. The mRNA amount was quantified according to the comparative Ct method with the $2^{-\Delta\Delta Ct}$ formula. The Ct values of GαS (endogenous control) were subtracted from the Ct values of the target gene (ΔCt). The mean of ΔCt of the reference (mainly WT or DMSO-treated controls) was then subtracted from each single ΔCt resulting in the $\Delta\Delta Ct$ value. The formula $2^{-\Delta\Delta Ct}$ provides the amount of mRNA in every sample.

2.2.3 Protein analysis

2.2.3.1 Protein extraction

For the measurement of the 20S activity, about 50 mg tissue powder (see 2.2.1) were mixed with 5 volumes of lysis buffer I (1 tablet complete mini protease inhibitor cocktail dissolved in 10ml aqua ad iniectabilia). After 3 cycles of freezing in liquid nitrogen and thawing at room temperature the samples were homogenized with Tissue Lyser twice for 30 sec at a frequency of 20 Hz. After centrifugation (13200 rpm, 30 min, 4°C), the supernatant was collected and its concentration was determined. For Western blot analysis, the above resulting pellet was resuspended in 5 volumes of Lysis Buffer II (3% SDS, 30 mM Tris base, pH 8.8, 5 mM EDTA, 30 mM NaF, 10% glycerol) and homogenized with the Tissue Lyser twice for 30 sec at a frequency of 30 Hz. After centrifugation (13200 rpm, 10 min, room temperature), the supernatant was collected and its concentration was determined as

described in the next chapter.

2.2.3.2 Determination of protein concentration

The protein concentration was determined by the Bradford protein assay, which is a dye-binding assay in which a differential color change of a dye occurs in response to various concentrations of protein (Bradford, 1976). For determination, 5 μ l of supernatant of protein samples were added to 795 μ l 0.1 M NaOH. After admixture of 200 μ l Coomassie[®] Brilliant Blue G-250 reagent and incubation at room temperature for 5 min, the absorbance at 595 nm was measured with a spectrophotometer. Subtraction of the blank value (800 μ l 0.1 M NaOH plus 200 μ l Coomassie[®] Brilliant Blue G-250 reagent) and comparison to a standard (immunoglobulin G) curve provided a relative measurement of protein concentration. Each protein concentration determination was performed in duplicates.

2.2.3.3 Western Blot analysis

Forty to 60 μ g of protein were adjusted to Laemmli buffer composition (2% SDS, 10% glycerol, 10 mM Tris base, pH 6.8, 100 mM DTT and 0.01% bromophenol blue), denatured by heating at 95 °C for 5 min and subsequently separated on 10% or 15% (depending on the target protein) polyacrylamide gels (running gel composition: 375 mM Tris base, pH 8.8, 10% or 15% acrylamide/bis solution (29:1), 0.1% SDS, 0.1% APS, 0.03% TEMED; stacking gel composition: 125 mM Tris base, pH 6.8, 5% acrylamide/bis solution (29:1), 0.1% SDS, 0.1% APS, 0.08% TEMED) by gel electrophoresis. Electrophoresis was carried out first at 80 V for 10 min and then at 150 V as long as needed in electrophoresis buffer (25 mM Tris base, 192 mM glycine, 0.1% SDS) using the Mini Protean 3 electrophoresis system. The Precision Plus Protein Standard[™] was used as molecular weight marker. After separation, the proteins were transferred onto a nitrocellulose membrane at 300 mA for 90 min in transfer buffer (50 mM Tris base, 380 mM glycine, 0.1% SDS, 20% methanol) using the Mini Trans-Blot cell system. Afterwards, the membrane was stained with Ponceau S to visualize the transferred proteins. After 3 times washing with TBS-T buffer (100 mM Tris base, pH 7.5, 150 mM NaCl, 0.1% Tween 20), the membrane was blocked in 5% milk solution (milk powder in TBS-T buffer) for 1 h at room temperature and then, after repeated washing, incubated with the primary antibody overnight at 4 °C. After 3 times washing with TBS-T buffer, the membrane was then incubated with the secondary antibody for 1 h at room temperature. After a final washing with TBS-T buffer, the membrane was incubated with a detection reagent according

to the instruction manual of the ECL Plus Western blotting detection system for tissue preparations or the SuperSignal[®] West Dura extended duration substrate for cell preparations. The produced chemiluminescent signal was detected with the Chemie Genius 2 Bio Imaging System and quantified with the Gene Tools software.

Table 2.4: Antibodies used for protein analysis in tissue.

Protein	Primary antibody	Dilution	Secondary antibody	Dilution
Calsequestrin	CSQ	1:2500	anti-rabbit IgG peroxidase conjugate	1:6000
GAPDH	GAPDH	1:2000	anti-rabbit IgG peroxidase conjugate	1:10000
GRP78	GRP78	1:1000	anti-rabbit IgG peroxidase conjugate	1:6000
GFP	GFP	1:2000	anti-rabbit IgG peroxidase conjugate	1:10000
IRE1 α	IRE1 α	1:1000	anti-rabbit IgG peroxidase conjugate	1:6000
p-eIF2 α	p-eIF2 α	1:1000	anti-rabbit IgG peroxidase conjugate	1:6000

The primary antibodies against calsequestrin, GAPDH, GFP and IRE1 α were diluted in TBS-T buffer, whereas the antibodies against GRP78 and IRE1 α were diluted in 5% BSA. The secondary antibodies were diluted in 5% milk solution.

2.2.3.4 Measurement of the 20S-proteasome activity

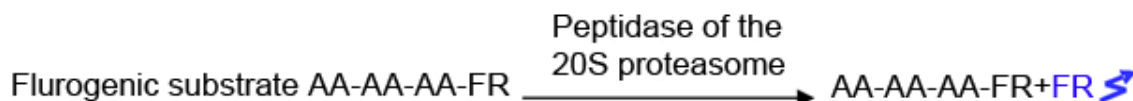


Figure 2.4: To measure the different activities of the 20S proteasome, specific fluorogenic substrates were used, which are composed of a chain of amino acids (AA) and a fluorescent reporter (FR). After cleavage of these substrates by a specific peptidase, the fluorescent reporter is released, whose fluorescence can be measured.

To measure the chymotrypsin-like activity of the proteasome, a specific fluorogenic substrate was used, which is composed of a chain of amino acids (AA) and a fluorescent reporter (FR; Figure 2.4). After cleavage of this substrate by a specific peptidase, the fluorescent reporter is released, whose fluorescence can be measured. This method was adapted from (Ludwig

et al., 2005). For determination, 30 µg of protein were incubated in the dark for 1 h at 37 °C in an incubation buffer (225 mM Tris-HCl, pH 8.2, 45 mM KCl, 7.5 mM Mg(CH₃COO)₂·4H₂O, 7.5 mM MgCl₂·6H₂O, 1.1 mM DTT) containing an ATP regenerating system (6 mM ATP, 5 mM phosphocreatine, 0.2 U phosphocreatinekinase) and the specific fluorogenic substrate (Table 2.5). Released fluorescence of the fluorescent reporter 7-amino-4-methylcoumarin (AMC) was measured using the TECAN Safire² microplate reader at an excitation wavelength of 380 nm and an emission wavelength of 460 nm. Each sample was measured in triplicates. The mean of the blank (incubation buffer and H₂O) was subtracted from the mean of each sample triplicate.

Table 2.5: Fluorogenic substrate used to measure chymotrypsin-like activity.

20S activity	Fluorogenic substrate	Concentration (µM)
Chymotrypsin-like activity	Succinyl-leucyl-leucyl-valyl-tyrosyl-7-amino-4-methylcoumarin (SUC-Leu-Leu-Val-Tyr-AMC)	60

2.2.4 Cell culture analysis

2.2.4.1 Neonatal mouse cardiomyocytes

Isolation of Neonatal mouse cardiomyocytes (NMCM) was performed by Dr. Saskia Schlossarek. Cells were isolated from at least 19 1-4 d-old mice according to a procedure adapted from (Laugwitz et al., 2005). Organ extraction from neonatal mice was authorized by the Behörde für Soziales, Familie, Gesundheit und Verbraucherschutz der Freien und Hansestadt Hamburg (Org 366). Neonatal mice were sacrificed by cervical dislocation. Mouse ventricles were removed aseptically, kept in a Ca²⁺/Mg²⁺-free HBSS on ice, washed, minced into small fragments in HBSS, and incubated overnight at 4 °C in 0.5 mg/ml trypsin-HBSS. This trypsin predigestion was followed by five rounds of digestion with 240 U/ml collagenase type II in HBSS solution at 37 °C for 9 min. Cells were collected in an equal volume of cold dark medium (DMEM:M199 3:1, 10% horse serum, 5% FCS, 100 U/ml penicillin-streptomycin, 1 mM HEPES, pH 7.4). The resulting mixture was centrifuged twice (8 and 5 min) at 600 rpm at room temperature and the cells were resuspended in 20-25 ml of dark medium. To exclude nonmuscle cells, the isolated cells were pre-plated twice in T75 flasks at 37 °C and 10% CO₂ for 75 min. All unattached cells, which were mainly cardiomyocytes, were transferred to a Falcon tube and spun again twice at 320 rpm for 5

min at room temperature before they were counted using a Neubauer chamber. NMCM were plated on laminin-coated (0.01 mg/ml; in 1x PBS) 12-well dishes at a density of 10^5 cells/cm² and incubated at 37 °C and 10% CO₂ for 4 d in the dark medium before treatment

2.2.4.2 Treatment of neonatal mouse cardiomyocytes

Provided WT and KI NMCM were plated on laminin-coated (0.01 mg/ml; in 1x PBS) 12-well dishes at a density of 10^5 cells/cm² and incubated at 37 °C and 10% CO₂ for 4 d in the dark medium (DMEM:M199 3:1, 10% horse serum, 5% FCS, 100 U/ml penicillinstreptomycin, 1 mM HEPES, pH 7.4) before treatment.

First two groups of NMCM were treated for 24 h with either 0.01 μM or 0.1 μM Tunicamycin in 0.1% DMSO-containing dark medium at 37 °C and 10% CO₂ for UPR induction. Groups three and four were treated for 24 h with either 0.01 μg/ml or 0.1 μg/ml Thapsigargin in 0.1% DMSO-containing dark medium at 37 °C and 10% CO₂. To rule out influence of the solvent, one group was cultured in the same way in 0.1% DMSO-containing dark medium only. Another group was cultured in dark medium only at 37 °C and 10% CO₂ and was therefore considered as untreated. Total RNAs were extracted from NMCM.

2.2.5 Statistical analysis

Data are presented as mean±SEM. Statistical analyses were performed using the unpaired Student's t-test or the analysis of covariance system (ANCOVA). Analyses were performed using commercial software (GraphPad Software, Inc.; SPSS, IBM Corp.). A value of $P < 0.05$ was considered significant.

3 Results

3.1 Evaluation of cardiac hypertrophy

A key feature of the used KI and KO mouse models is LVH. Therefore at the beginning of this investigation, we evaluated the heart-to-body-weight (HW/BW) and ventricular-to-body-weight (VW/BW) ratios in the three groups of animals, which were all crossed with Ub^{G76V}-GFP transgenic mice. KO mice were slightly older than respective WT. Yet there was no difference in the means of age between KO and KI mice (Figure 3.1A). The means of total body weight did not differ between KO/KI and respective WT (Figure 3.1C). HW/BW as well as VW/BW ratios were significantly higher in both KO and KI mice than in WT mice (Figure 3.1A; B). Hereby ventricular hypertrophy was confirmed for all animals used in the investigation.

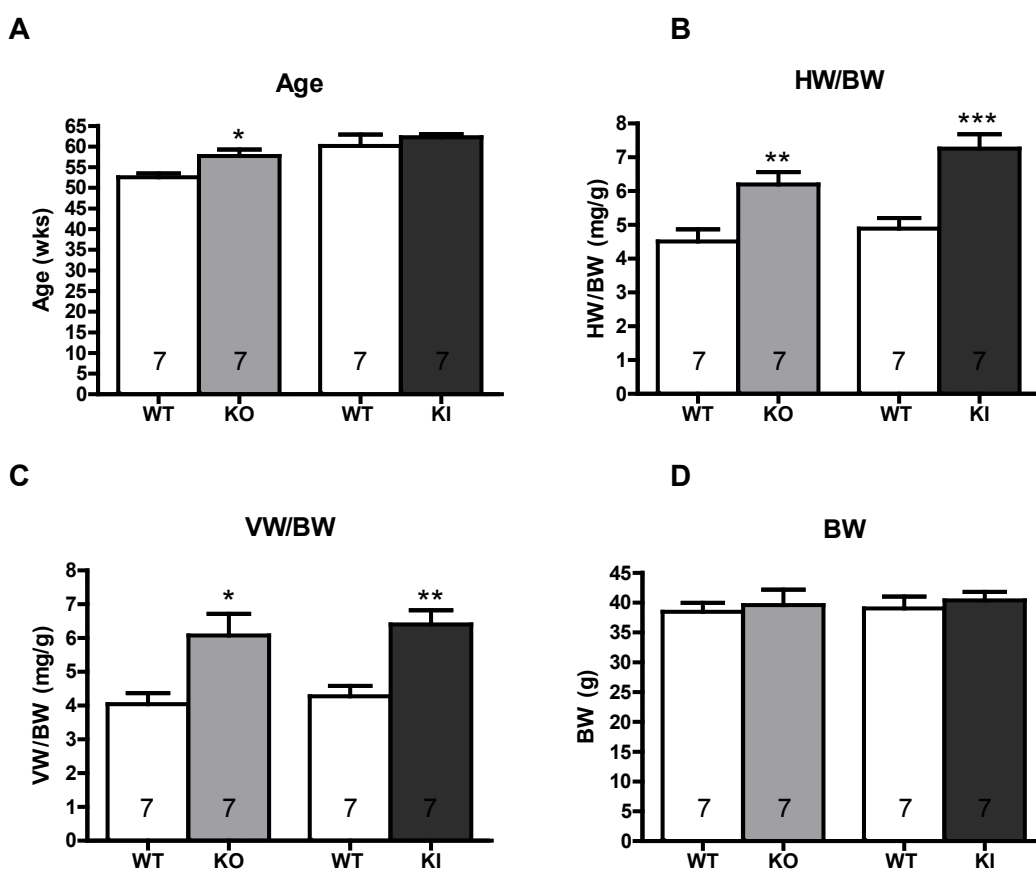


Figure 3.1: Cardiac phenotype of KO, KI and corresponding WT mice. Mice and extracted hearts of all animals were weighed to determine the means of heart weight to body weight ratios (A), the means of ventricular weight to body weight ratios (B) and the means of body weight (C). All animals were between 50 and 60 weeks of age (D). Bars represent the mean \pm SEM, *P<0.05, **P<0.01 and ***P<0.001 vs. WT, Student's t- test. The number of animals was n=7, as indicated within the bars.

3.2 Evaluation of protein degradation

Both mouse models carry a mutant *Mybpc3* allele at the homozygous state. KI mice exhibit LVH with reduced fractional shortening and express low levels of mutant cMyBP-C (10% of normal). The reduction in cMyBP-C results from activation of both NMD and the ubiquitin-proteasome system (Vignier et al., 2009). KI mice were compared to homozygous KO exhibiting a similar phenotype, but do not express any cMyBP-C thus serving as a pure model of cMyBP-C insufficiency. As discussed in 1.6, due to previous results, we expected that distractions in protein metabolism caused by mutant proteins, which need to be degraded, might be capable to trigger the UPR. In order to analyze protein degradation, Ub^{G76V}-GFP protein- and mRNA levels, as well as the chymotrypsin-like UPS activity were determined (see 1.3).

3.2.1 Determination of Ub^{G76V}-GFP protein levels

Protein levels of Ub^{G76V}-GFP were determined by Western Blot according to 2.2.3.3. Ub^{G76V}-GFP serves as an activity reporter for protein degradation by the ubiquitin-proteasome system. In case of regular function, a low level of Ub^{G76V}-GFP should be detected. In contrast, upon inhibited or impaired global proteolytic capacity Ub^{G76V}-GFP protein levels should be higher. The measurement revealed no significant difference between KO and respective WT mice. KI animals exhibited 4-fold higher Ub^{G76V}-GFP protein levels (Figure 3.2) suggesting impaired UPS activity and protein accumulation.

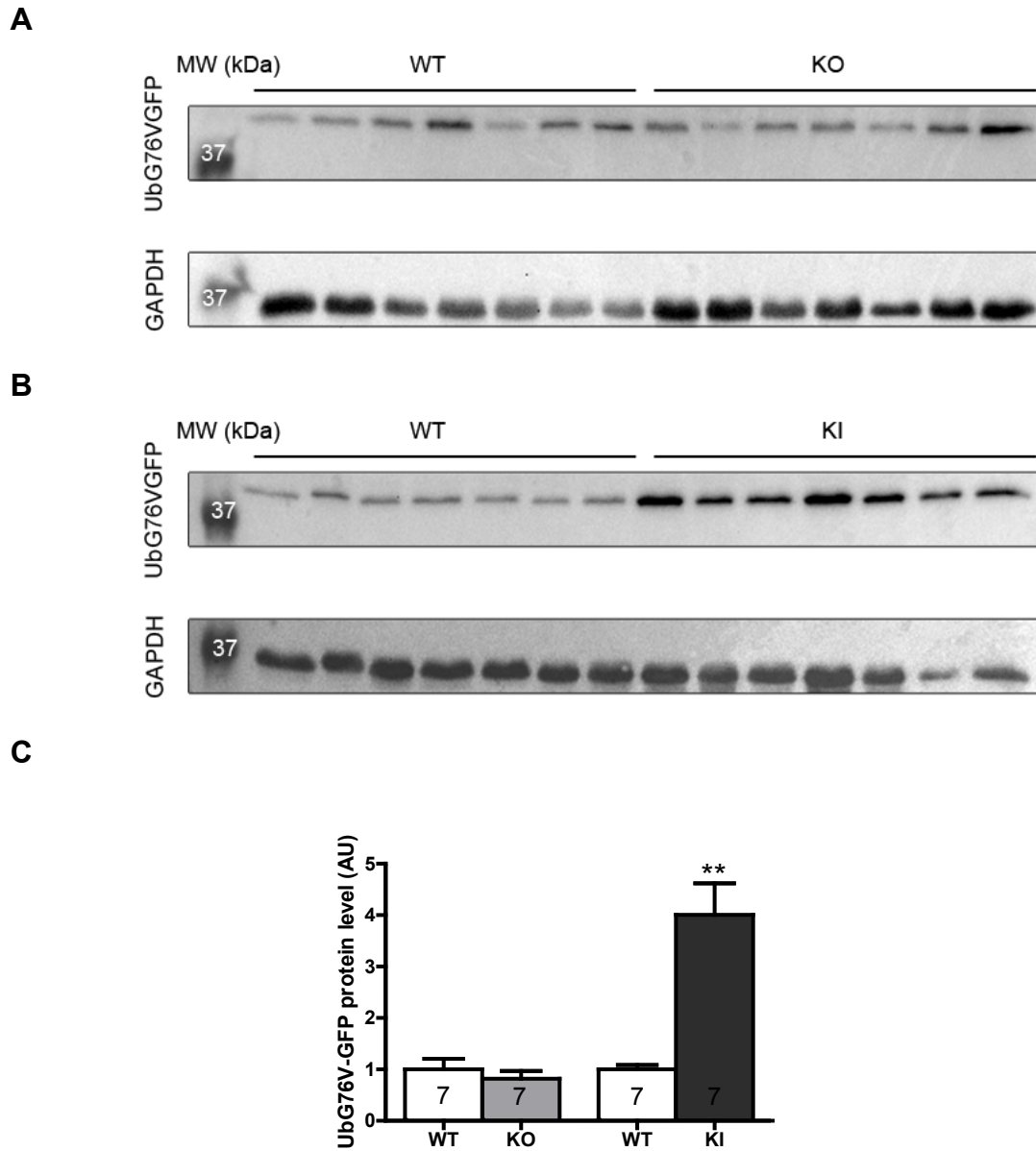


Figure 3.2: Determination of Ub^{G76V}-GFP protein levels in KO, KI and WT mice. Proteins were extracted from the ventricles of about 60 week-old KO (**A**) and KI (**B**) mice and their respective WT. Western Blots on top were stained with an antibody against GFP. Below, Western Blots were stained with an antibody against GAPDH. MW stands for molecular weight marker. (**C**) Bars represent the quantitative analysis normalized to GAPDH and related to WT. Data is shown as mean±SEM with ** $P < 0.01$ vs. WT, Student's t-test. The number of animals is indicated in the bars.

3.2.2 Determination of Ub^{G76V}-GFP mRNA levels

To rule out that higher Ub^{G76V}-GFP protein levels are due to increased transcription, mRNA levels of Ub^{G76V}-GFP were determined by RT-qPCR using the SYBR[®] Green strategy (see 2.2.2.4). As an internal standard GαS was used. The different expression levels are shown in Figure 3.3. The measurement revealed no significant differences between the groups, supporting the view that Ub^{G76V}-GFP protein accumulation due to higher expression rates seems unlikely and is rather due to defective protein degradation.

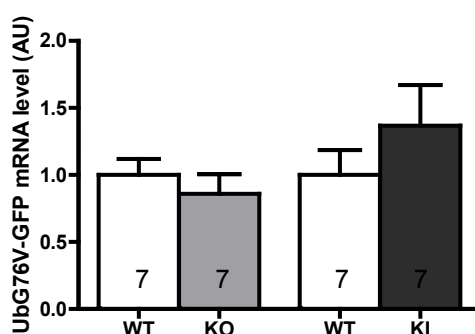


Figure 3.3: Determination of the level of Ub^{G76V}-GFP mRNA in KO, KI and WT mice. Total RNA was reversed transcribed to cDNA and amplified by PCR using specific primers. GαS was used as an endogenous control. Bars represent the mean±SEM. The number of animals is indicated in the bars.

3.2.3 Evaluation of the chymotrypsin-like activity

Potential differences in the enzymatic activity of the ubiquitin-proteasome system were investigated by measuring its chymotrypsin-like activity, which is the main activity of the proteasome. It was determined in ventricular cytosolic extracts of KO, KI and respective WT mice according to 2.2.3.4. A trend to lower activity in KI than WT was noticed ($p=0.08$), yet suggesting decreased activity in KI. The activity was lower in KI than in KO ($p<0.05$).

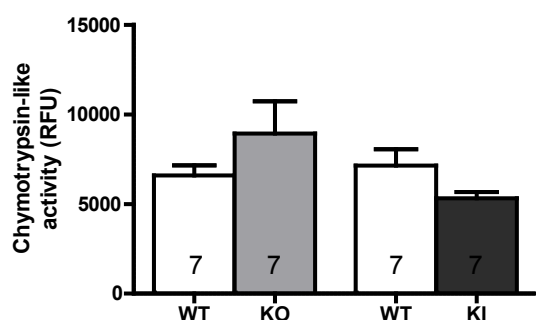


Figure 3.4: Chymotrypsin-like activity of the proteasome in KO, KI and WT hearts. Ventricular cytosolic proteins were extracted from the same heart tissue used in previous investigations. Bars represent the mean±SEM. Number of animals is indicated in the bars.

3.2.4 Summary

The major findings of this part were the following:

- KI mice exhibited 4-fold higher protein levels of Ub^{G76V}-GFP than WT mice, whereas there was no difference between KO and respective WT.
- There was no difference detected in Ub^{G76V}-GFP mRNA levels in KO/KI compared to WT.
- The chymotrypsin-like activity was not significantly lower in KI vs WT, whereas it was much lower in KI than in KO.

In combination these results suggest an impairment of the ubiquitin-proteasome system in 1-year-old KI carrying a HCM mutation, but not in KO mice.

3.3 Evaluation of the unfolded protein response in KO and KI mice

Fundamental UPR factors were evaluated to detect a potential UPR activation in KI and KO mice due to disturbances in the protein metabolism caused by mutant cMyBP-C proteins. Especially in KI mice, an eventual activation of the UPR due to the impairment of the UPS with age was investigated in detail.

3.3.1 Qualitative PCR analysis

In order to prove functionality and gain amplification products for sequencing, all primers were tested by classical RT-PCR and amplicons were validated by sequencing (data not shown). Interestingly, despite of normalized RNA amounts used for reversed transcription, classical RT-PCR (though not a quantitative method) revealed considerable differences in the amount of amplification products between the WT and KI group. Figure 3.5 shows GRP78 PCR amplification as an example. The levels of GRP78 mRNA were obviously lower in KI than in WT mice. No bands were amplified in the controls (H₂O and RNA samples without reverse transcription).

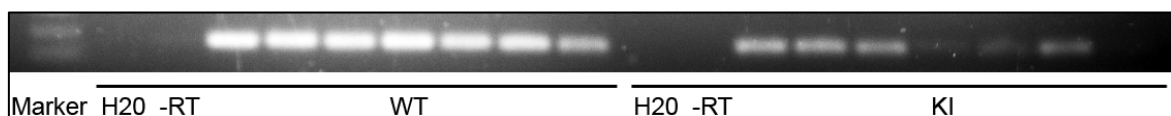


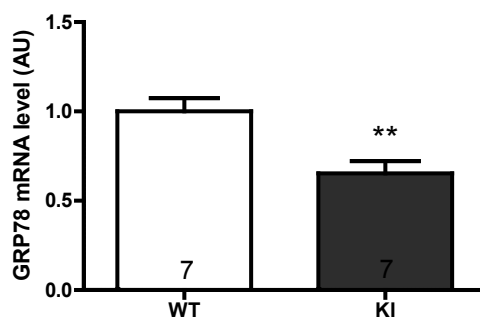
Figure 3.5: Qualitative PCR analysis of GRP78 expression. Total RNA isolated from ventricles was reversed transcribed to cDNA. Approaches without adding the reverse transcriptase are indicated as -RT. H₂O corresponds to control using water instead of RNA. PCR was performed using primers for GRP78 (see 2.2.2.2).

3.3.2 Evaluation of the UPR trigger GRP78

3.3.2.1 Determination of GRP78 mRNA levels

Due to its fundamental function within all pathways, the investigation of the UPR was started by determining the mRNA levels of GRP78 in KI mice. Contrary to our expectations the measurement revealed a ~30% lower GRP78 mRNA level in KI than in WT (Figure 3.6A). The analysis was repeated using GαS as an endogenous control, to rule out a bias due to a potentially altered GAPDH expression. The second analysis confirmed the previous result independent from the respective endogenous control.

A



B

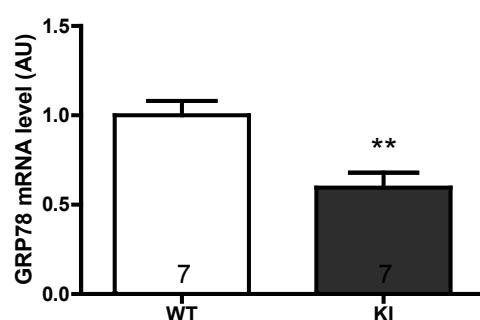


Figure 3.6: Determination of GRP78 mRNA levels in KI and WT mice. (A) Total RNA was reversed transcribed to cDNA and amplified by quantitative PCR using specific primers. *GAPDH* was used as an endogenous control. (B) *GαS* was used as an endogenous control. The number of animals is indicated in the bars. Bars represent the mean±SEM with ** $P < 0.01$ vs. WT, Student's t-test.

Since these early results contradicted our expectations, we decided to include the KO mouse model in all further UPR evaluations to be able to compare the influence of the respective genotype. Therefore the measurement was repeated a third time including the KO animals. This third analysis (Figure 3.7) confirmed all previous results with respect to the KI group, while there was no difference detected between the KO and WT group.

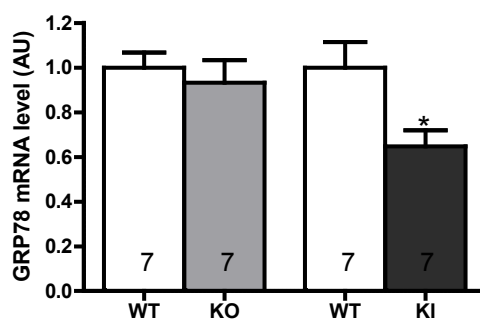
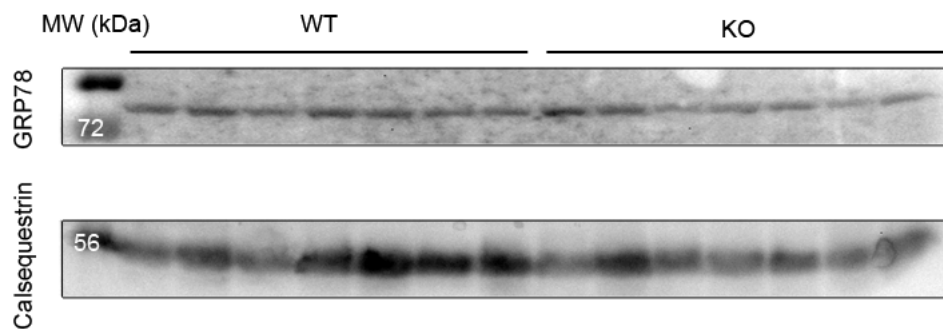


Figure 3.7: Determination GRP78 mRNA levels in KO, KI and WT mice. *GαS* was used as an endogenous control. The number of animals is indicated in the bars. Bars represent the mean±SEM with * $P < 0.05$ vs. WT, Student's t-test. Measurement done by Saskia Schlossarek.

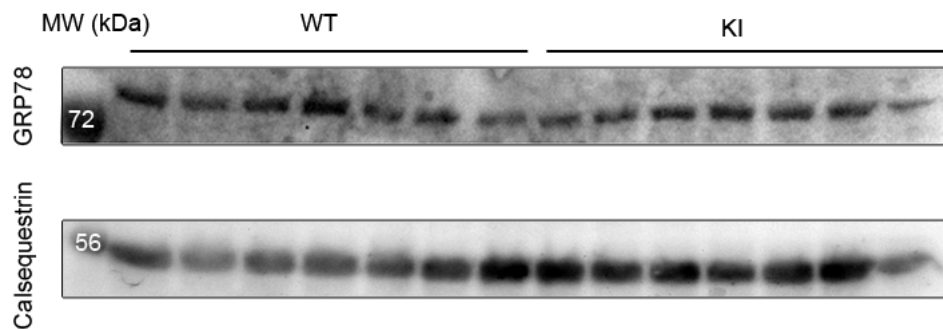
3.3.2.2 Evaluation of GRP78 protein levels

GRP78 protein levels were determined by Western Blot according to 2.2.3.3. The measurement revealed no significant differences between the groups, but exhibited a slight, non-significant lower GRP78 protein level in KI animals (Figure 3.8). However, a larger amount of calsequestrin in KI mice could explain these lower levels. Therefore this measurement did not support the previously determined lower mRNA levels of GRP78 in KI.

A



B



C

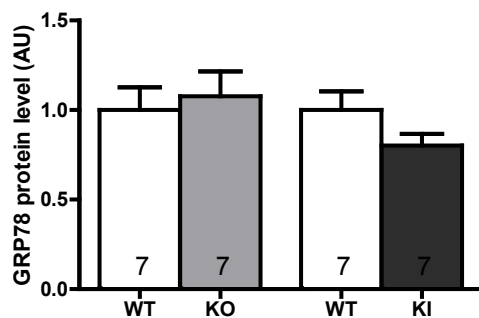


Figure 3.8: Determination of GRP78 protein levels in KO and KI mice. Proteins were extracted from about 60 week-old KO (**A**) and KI (**B**) mice and their respective WT. Western Blots on top were stained with an antibody against GRP78. Below, Western Blots were stained with an antibody against calsequestrin. (**C**) Quantification of GRP78 protein levels. Bars represent the quantitative analysis normalized to calsequestrin and related to WT. MW stands for molecular weight marker. Bars represent the mean \pm SEM. The number of animals is indicated in the bars.

3.3.3 Evaluation of the IRE1 α pathway

3.3.3.1 Determination of IRE1 α protein levels

Protein levels of IRE1 α were determined by Western Blot according to 2.2.3.3 in order to evaluate potential up-regulation of the receptor at this early point of the pathway (Figure 3.9). Quantification revealed ~ 1.7-fold higher levels of IRE1 α in KO than in WT. On the other hand, the IRE1 α protein levels did not differ between KI and WT mice (Figure 3.10; Figure 3.11). These data suggest activation of the IRE1 α pathway in KO but not in KI. However we cannot rule out that the phosphorylation level of IRE1 α , which has not been measured here, is lower in KI.

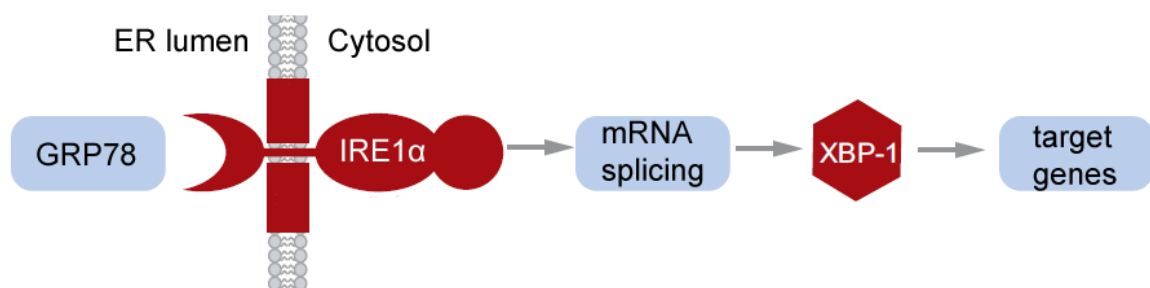


Figure 3.9: IRE1 α receptor within the pathway (adapted from Ho, 2009). IRE1 α is the most fundamental ER stress sensor (Tirasophon et al., 1998). Its activation is followed by dimerization and autophosphorylation which enables downstream-signaling via XBP-1.

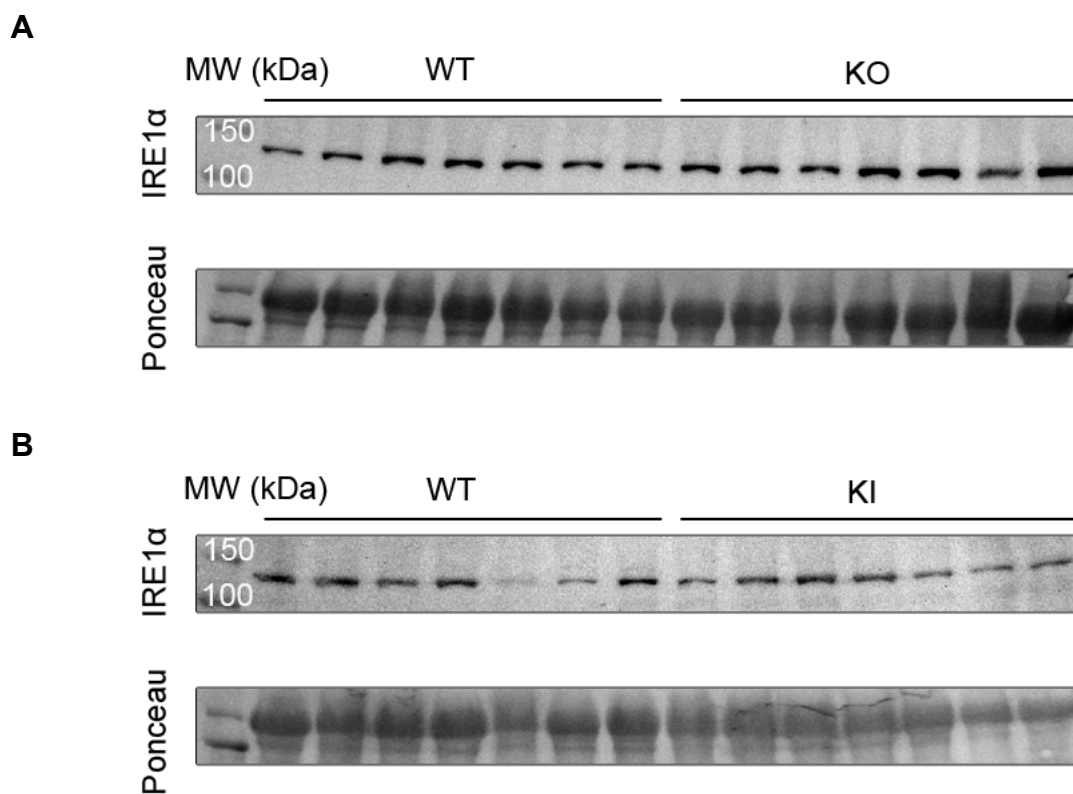


Figure 3.10: Determination of IRE1 α protein levels in KO and KI mice. Proteins were extracted from about 60-week-old KO (A) and KI (B) mice and their respective WT. Western Blots on top were stained with an antibody against IRE1 α . Below each blot the corresponding Ponceau is shown. Measurement done by Saskia Schlossarek.

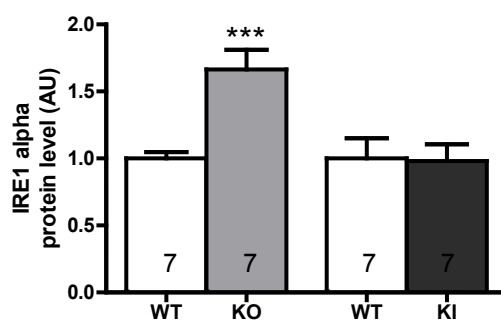


Figure 3.11: Quantification of IRE1 α protein levels. Bars represent the quantitative analysis normalized to Ponceau and related to WT. MW stands for molecular weight marker. Data Bars represent the mean \pm SEM with *** P <0.001 vs. WT, Student's t-test. The number of animals is indicated in the bars.

3.3.3.2 Determination of XBP-1 mRNA levels

Upon UPR activation, XBP-1 mRNA is spliced and only hereby capable to be transcribed into the active XBP-1 protein (see Figure 3.9). XBP-1 transcript levels were analyzed in KO and KI mice using specific Taqman probes, recognizing either the unspliced and inactive or the spliced active mRNA (see 2.2.2.4; see Figure 3.12A and B). While the expression levels of the unspliced XBP-1 did not differ between the groups, the level of spliced XBP-1 mRNA was ~ 50% lower in KI mice than in WT mice and 90% higher in KO than in WT mice. These data support the view of activation and inhibition of the IRE1 α pathway in KO and KI, respectively.

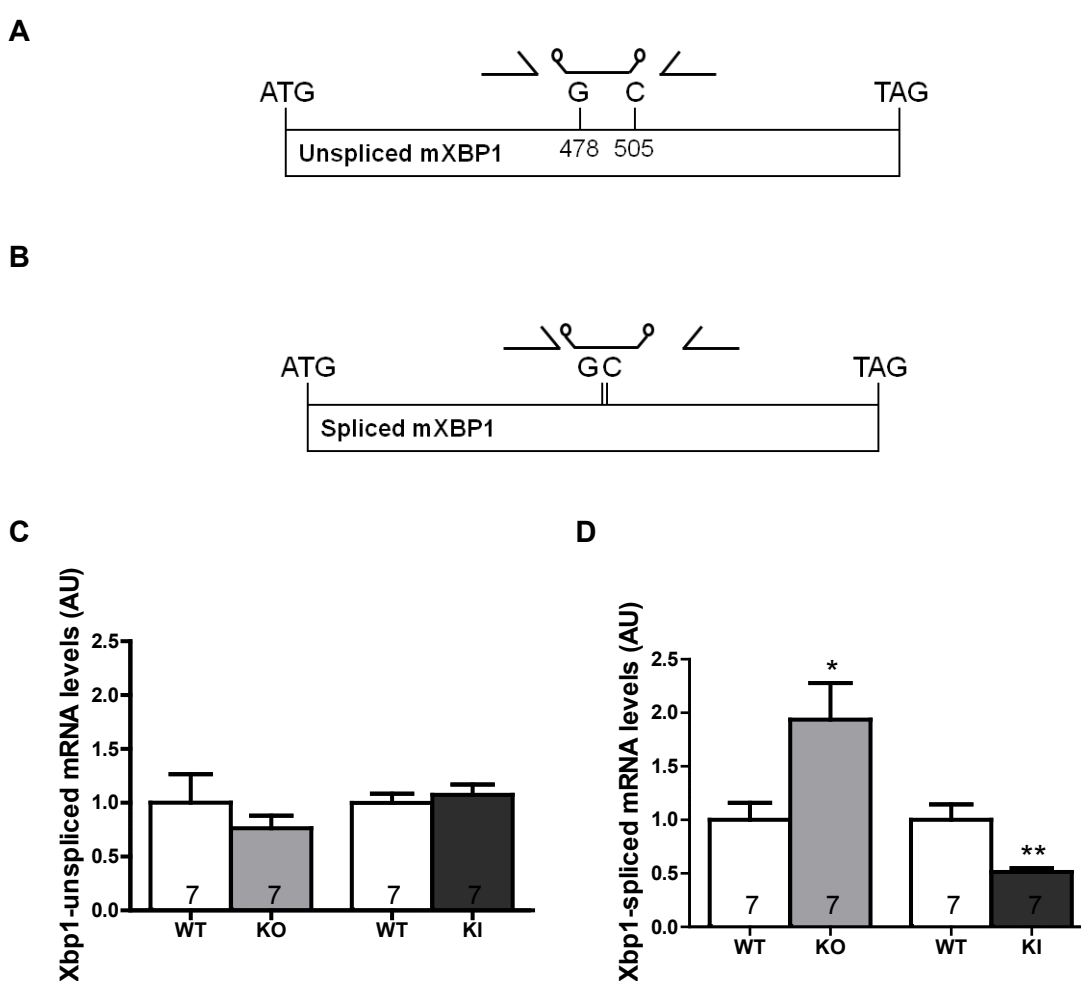


Figure 3.12: Taqman probes and results of Xbp-1 mRNA evaluation. (A) Taqman probe used to detect *unspliced* XBP1 mRNA levels. (B) Probe for *spliced* Xbp-1 mRNA levels. (C) Levels of *unspliced* XBP-1 mRNA in KO, KI and WT mice. (D) Levels of *spliced* Xbp-1 mRNA in KO, KI and WT mice. Total RNA was reverse transcribed to cDNA and amplified by quantitative PCR using specific primers and specific taqman probes. GaS was used as an endogenous control. The number of animals is indicated in the bars. Bars represent the mean \pm SEM with * P <0.05 and ** P <0.01 vs. WT, Student's t-test.

3.3.4 Evaluation of the ATF6 pathway: CHOP and Bcl-2 mRNA levels

Since the regulation of cellular apoptosis is the second pathway's decisive function, the transcript levels of pro-apoptotic CHOP and anti-apoptotic Bcl-2 were analyzed in KO and KI mice according to 2.2.2.4. Measurement was performed equally as in 3.2.2 using the same RNA. The measurement revealed no significant differences in CHOP or Bcl-2 in both KO and KI compared to WT (Figure 3.13). Although protein levels of ATF6 were not determined, these results suggest no activation of apoptosis in both mutant mouse models.

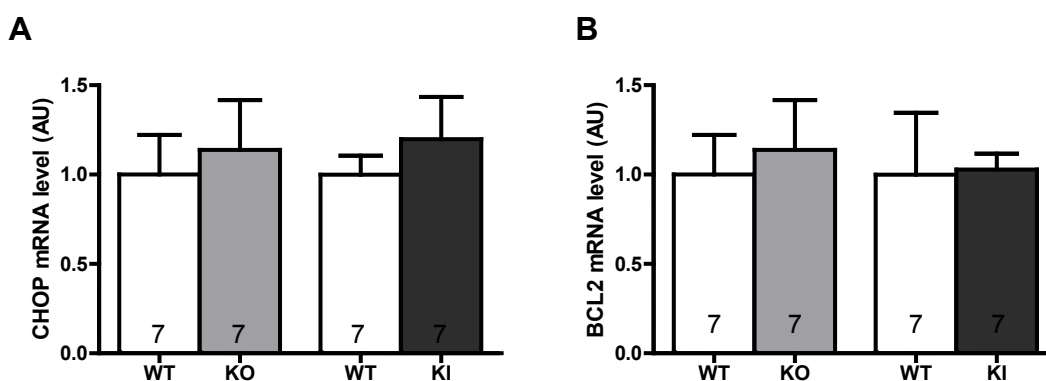


Figure 3.13: Determination of the level of CHOP (A) and Bcl-2 (B) mRNA in KO, KI and WT mice. Total RNA was reversed transcribed to cDNA and amplified by quantitative PCR using specific primers. GαS was used as an endogenous control. The number of animals is indicated in the bars. Bars represent the mean ± SEM.

3.3.5 Evaluation of the PERK pathway

Upon activation, the receptor protein PERK is capable to phosphorylate eIF2α which activates downstream signaling (Figure 1.5).

3.3.5.1 Determination of eIF2α phosphorylation level

To evaluate the activity of the third pathway, levels of phosphorylated eIF2α (p-eIF2α) were determined. The measurement revealed no significant differences in the protein levels of KO, KI and respective WT (Figure 3.14).

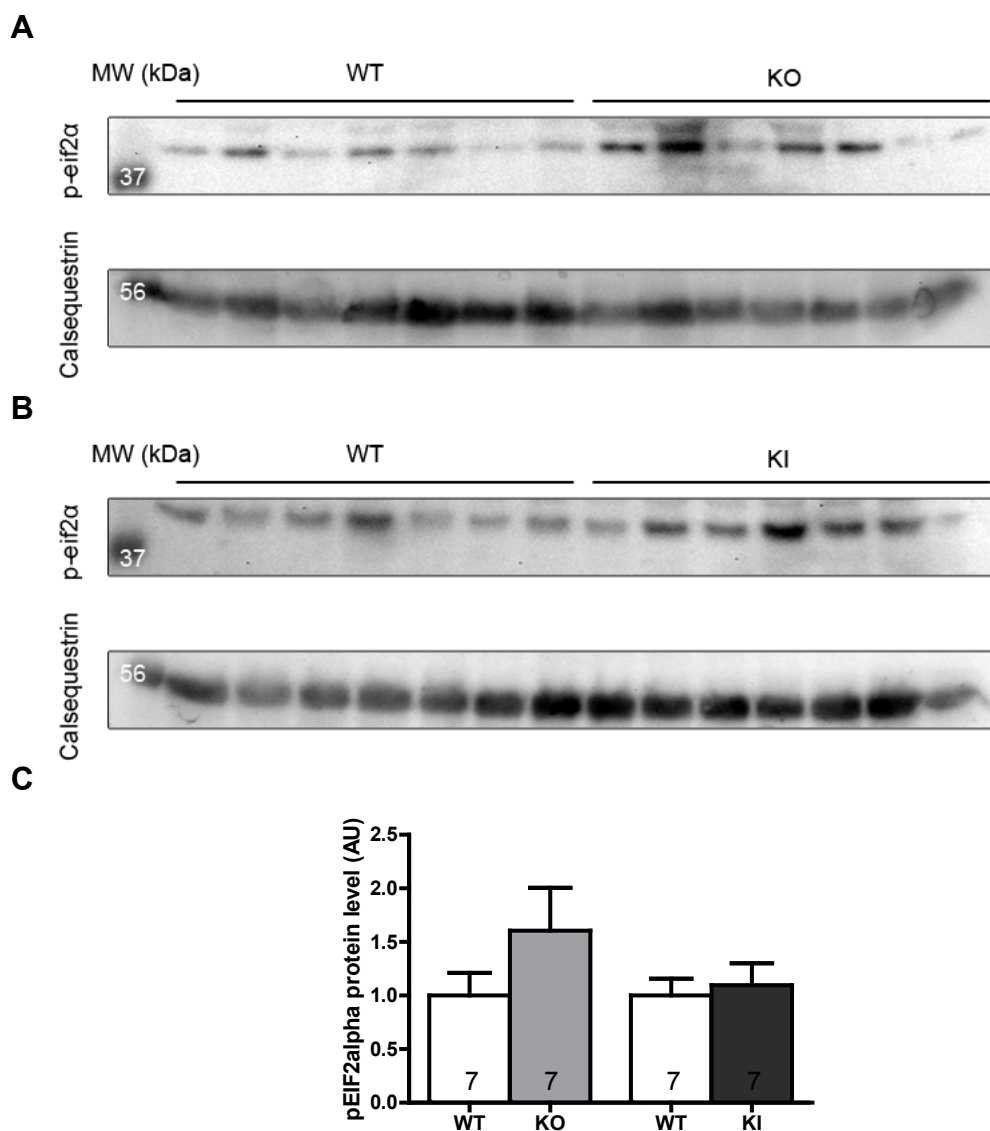


Figure 3.14: Determination of p-eIF2 α protein levels in KO and KI mice. Proteins were extracted from about 60 week-old KO (**A**) and KI (**B**) mice and their respective WT. Western Blots on top were stained with an antibody against IRE1 α . Below each Blot the corresponding Ponceau is shown. Below, Western Blots were stained with an antibody against calsequestrin. (**C**) Quantification of p-eIF2 α protein levels. Bars represent the quantitative analysis normalized to calsequestrin and related to WT. Bars represent the mean \pm SEM. The number of animals is indicated in the bars.

3.3.5.2 Determination of ATF4 mRNA levels

Though predominantly regulated at protein level, increased ATF4 mRNA levels were also reported in cases of UPR induction (Fu et al., 2010; Magne et al., 2011). Therefore mRNA levels were determined for all animals to gain further insights in the PERK pathway. The measurement revealed no significant differences between any of the groups, except for a non-significant increase in ATF4 mRNA in KO mice (Figure 3.15).

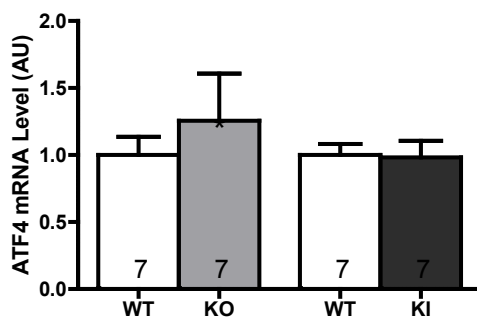


Figure 3.15: Determination of the level of ATF4 mRNA in KI and WT mice. Total RNA was reversed transcribed to cDNA and amplified by quantitative PCR using specific primers. G α S was used as an endogenous control. The number of animals is indicated in the bars. Bars represent the mean \pm SEM.

3.3.6 Evaluation of chaperones' induction

Transcription of the chaperones calnexin, calreticulin and GRP94 is known to be influenced by the UPR (Kitakaze et al., 2010). To assess potential consequences of UPR activity on the chaperone's assistance to protein folding, their transcription levels were determined. No significant differences were detected (Figure 3.16).

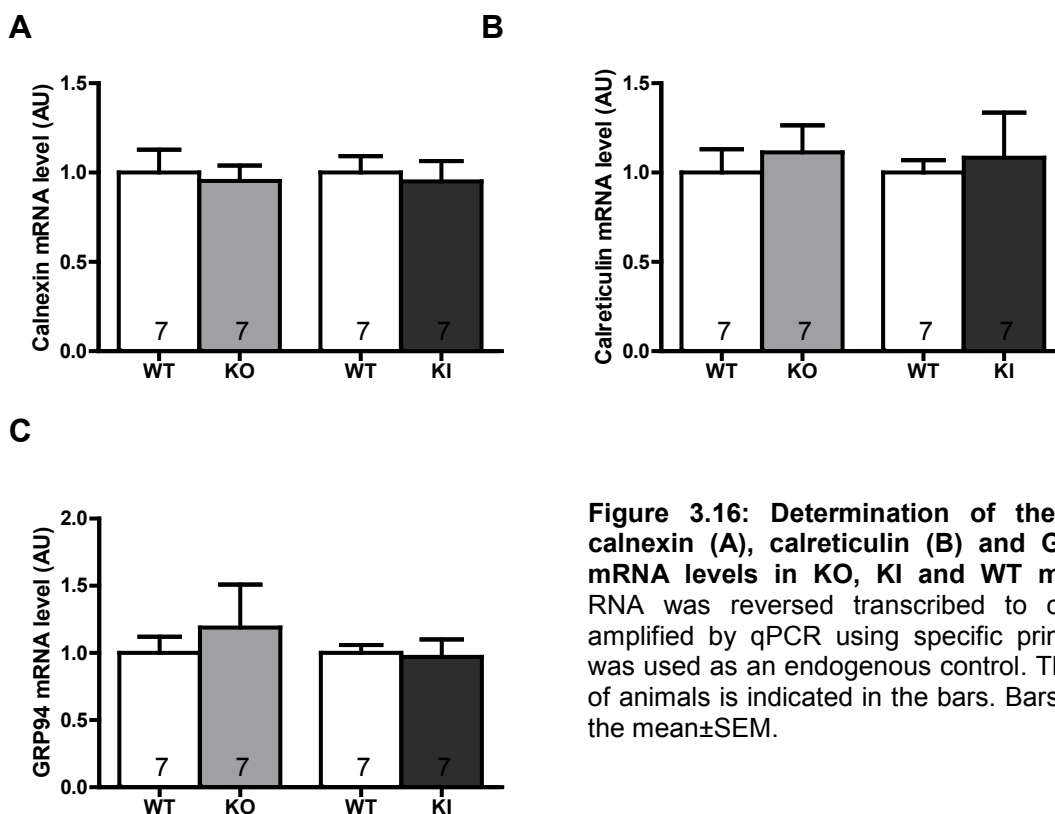


Figure 3.16: Determination of the level of calnexin (A), calreticulin (B) and GRP94 (C) mRNA levels in KO, KI and WT mice. Total RNA was reversed transcribed to cDNA and amplified by qPCR using specific primers. G α S was used as an endogenous control. The number of animals is indicated in the bars. Bars represent the mean \pm SEM.

3.3.7 Determination of oxidative stress antagonist Metallothionein-1

Metallothionein-1 (MT1) was demonstrated to be a powerful antagonist of oxidative stress and furthermore induced by the UPR (Bell et al., 2009). To investigate whether an induction due to oxidative stress is detectable we determined MT1 mRNA levels. The measurement revealed no significant differences in transcription of MT1 between the groups. This contradicts an adaptive increase of MT1 in order to antagonize potential higher levels of oxidative stress.

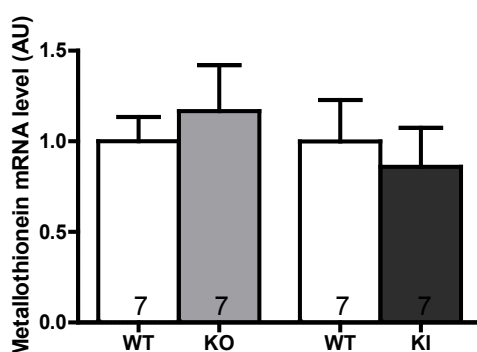


Figure 3.17: Determination of the level of Metallothionein-1 mRNA levels in KO, KI and WT mice. Total RNA was reverse transcribed to cDNA and amplified by qPCR using specific primers. G α S was used as an endogenous control. The number of animals is indicated in the bars. Bars represent the mean \pm SEM.

3.3.8 Evaluation of GRP78, CHOP and ATF4 at different time points in KI

To gain insights in the activity of the UPR at different animal ages, GRP78, CHOP and ATF4 mRNA levels were additionally determined in heart tissue samples of neonates (2-4-day-old) and 9-week-old KI and WT mice (Figure 3.18). RNA was extracted, reverse transcribed and amplified similarly as in all previous experiments. In neonatal KI mice GRP78 mRNA was \sim 25% lower than in WT, almost similar to previous measurements in 60-week-old. In 9-week-old WT mice GRP78 mRNA level was even \sim 70% lower than in WT. Considering all results, at any time point GRP78 levels were significantly lower in the KI model (Figure 3.19).

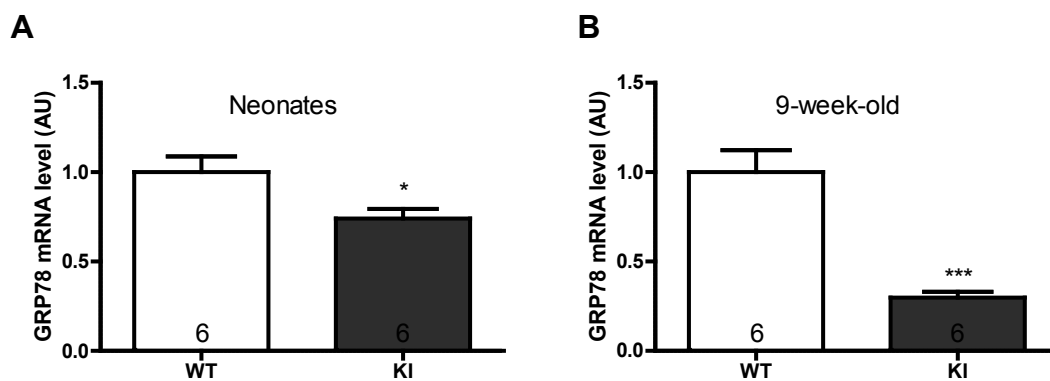


Figure 3.18: Determination of the level of GRP78 mRNA in 2-4-day-old (A) and 9-week-old (B) KI and WT mice. Total RNA was reversed transcribed to cDNA and amplified by quantitative PCR using specific primers. GαS was used as an endogenous control. The number of animals is indicated in the bars. Bars represent the mean±SEM with * $P < 0.05$ and *** $P < 0.001$ vs. WT, Student's t-test.

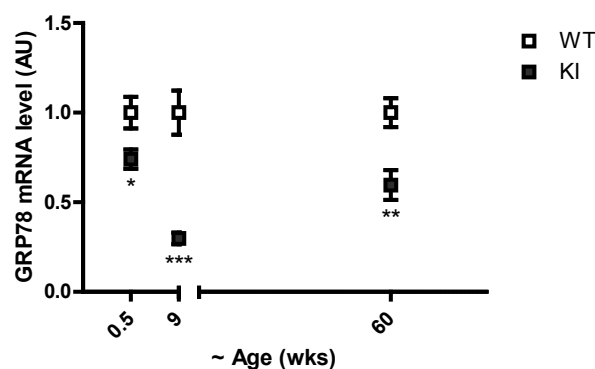


Figure 3.19: Overview of GRP78 mRNA levels from neonatal to 60-week-old KI and WT mice. Squares represent the mean±SEM with * $P < 0.05$, ** $P < 0.01$ and *** $P < 0.001$ vs. WT, Student's t-test.

In neonates CHOP mRNA was ~ 60% lower than in WT. In 9-week-old mice no significant difference could be detected anymore, as in 60-week-old KI and WT mice (Figure 3.20 and Figure 3.21).

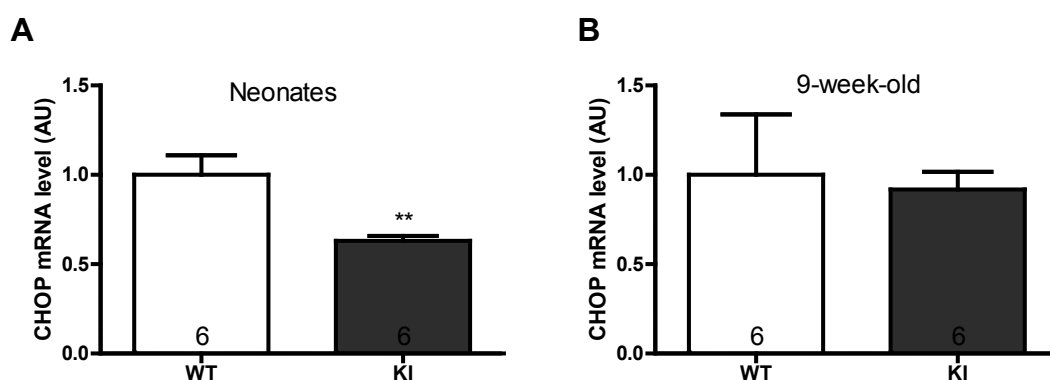


Figure 3.20: Determination of CHOP mRNA levels in 2-4-day-old (A) and 9-week-old (B) KI and WT mice. Total RNA was reversed transcribed to cDNA and amplified by quantitative PCR using specific primers. GαS was used as an endogenous control. The number of animals is indicated in the bars. Bars represent the mean±SEM with ** $P < 0.01$ vs. WT, Student's t-test.

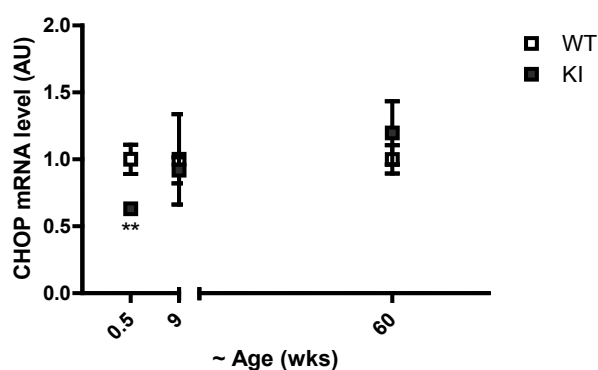


Figure 3.21: Overview of CHOP mRNA levels from neonatal to 60-week-old KI and WT mice. Squares represent the mean \pm SEM with ** P <0.01 vs. WT, Student's t-test.

For the ATF4 mRNA levels no significant difference between the groups was detected (Figure 3.22). Therefore no overview is shown here.

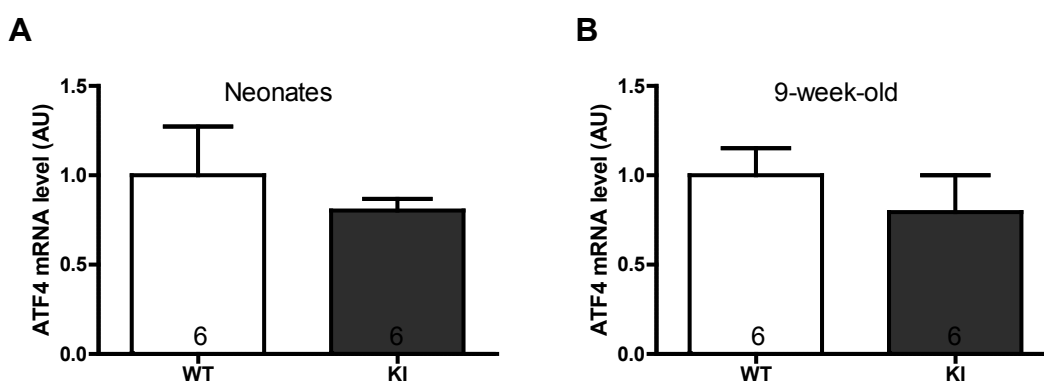


Figure 3.22: Determination of ATF4 mRNA levels in 2-4-day-old (A) and 9-week-old (B) KI and WT mice. Total RNA was reversed transcribed to cDNA and amplified by quantitative PCR using specific primers. G α S was used as an endogenous control. The number of animals is indicated in the bars. Bars represent the mean \pm SEM.

3.3.9 Summary

The major findings of this part were the following:

- In KO mice IRE1 α protein level was ~ 70% higher and spliced XBP-1 mRNA ~ 90% higher than in WT mice.
- In KI mice XBP-1 mRNA level was ~ 50% lower than in WT mice.
- In KI mice at three different time points GRP78 mRNA was significantly lower than in WT mice.

- In neonatal KI mice CHOP mRNA level was ~ 37% lower than in WT.

Together, these data suggest a defective UPR in KI mice, mainly of the first IRE1 α pathway, but an activated UPR in KO mice.

3.4 The unfolded protein response in neonatal mouse cardiomyocytes

3.4.1 Analysis of GRP78, XBP-1 and CHOP in KI and WT NMCM

To explore a potential UPR dysfunction in the KI mice due to aberrant proteins impairing the UPS, another experimental setting was used. KI-NMCM were cultured in order to force UPR induction by drug treatment. First of all the GRP78, spliced XBP-1 and CHOP mRNA levels were determined in cultures of untreated NMCM serving as a control groups. Total RNA was isolated from cells and reverse transcribed to cDNA. Levels were determined by quantitative RT-PCR using either the SYBR[®] Green strategy or specific TaqMan probes, as in previous experiments. The mRNA levels of GRP78, spliced XBP-1 and CHOP did not differ between KI- and WT-NMCM (Figure 3.23). These results were against expectations, at least regarding GRP78, which showed lower levels in 2-4-old KI hearts (Figure 3.18). Together these data suggest that a defective UPR is not revealed in cultured cardiomyocytes directly.

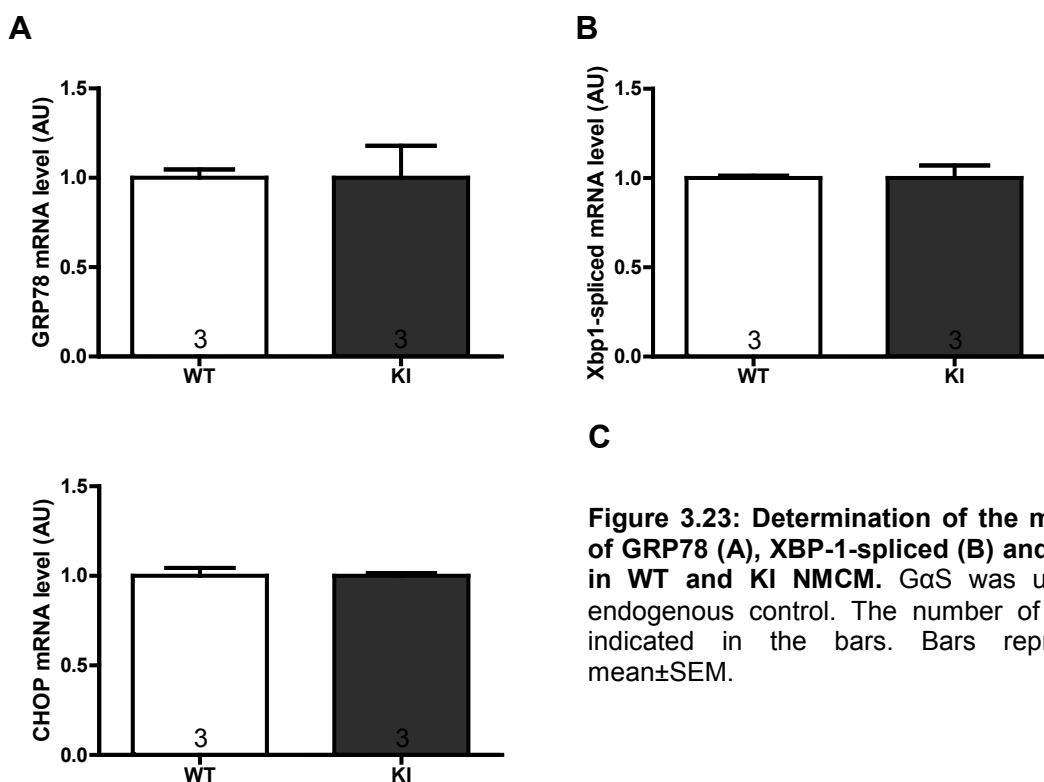


Figure 3.23: Determination of the mRNA level of GRP78 (A), XBP-1-spliced (B) and CHOP (C) in WT and KI NMCM. G α S was used as an endogenous control. The number of animals is indicated in the bars. Bars represent the mean \pm SEM.

3.4.2 Treatment of NMCM with UPR inducers tunicamycin and thapsigargin

After evaluation of the control groups GRP78, XBP-1 and CHOP mRNA levels were determined in cultured NMCM treated with different concentrations of tunicamycin and thapsigargin in order to investigate the outcome of a forced UPR induction. Tunicamycin is an inhibitor of N-glycosylation and hereby blocks glycoprotein synthesis (Iwata et al., 2005). Thapsigargin raises cytosolic Ca^{2+} concentration by blocking the endoplasmic reticulum Ca^{2+} ATPase (SERCA; Rogers et al., 1995). Both drugs reliably increase cellular ER stress and are used routinely for UPR induction. Cells were treated according to 2.2.4.1 with two different concentrations of tunicamycin or thapsigargin, as well as DMSO as a vehicle control.

3.4.2.1 Determination of GRP78 mRNA levels

While treatment with DMSO did not significantly influence the mRNA levels of GRP78 in both WT- and KI-NMCM, the effects of treatment with tunicamycin and thapsigargin were very well allocable. In WT-NMCM (Figure 3.24A), low concentration of tunicamycin did not reveal any effect. However, at 10-fold higher concentration the GRP78 mRNA level was ~ 4.7-fold higher than in the control group. Thapsigargin already influenced the expression at low concentration, causing a ~ 2.8-fold higher mRNA level. At higher concentration of thapsigargin GRP78 mRNA amounts were ~ 15-fold higher than in the control group. Generally, KI-NMCM (Figure 3.24B) exhibited a much higher variation of means with lower maxima of expression. At lower concentration, tunicamycin increased ~ 2.4-fold higher mRNA level, while there was no increase at higher concentration. Thapsigargin increased the level of GRP78 mRNA ~ 6-fold higher at low, and ~ 6.4-fold at high concentration. These data suggest that both WT- and KI-NMCM respond to ER stress by increasing mRNA levels of GRP78. In addition, whereas these levels increased by raising concentrations of tunicamycin and thapsigargin in WT, KI-NMCM exhibited a blunted effect at higher concentration of UPR inducers. Direct comparison of KI- and WT-NMCM both treated with high concentration thapsigargin, revealed that the increase of GRP78 mRNA is 2-fold lower in KI than in WT NMCM (Figure 3.24C).

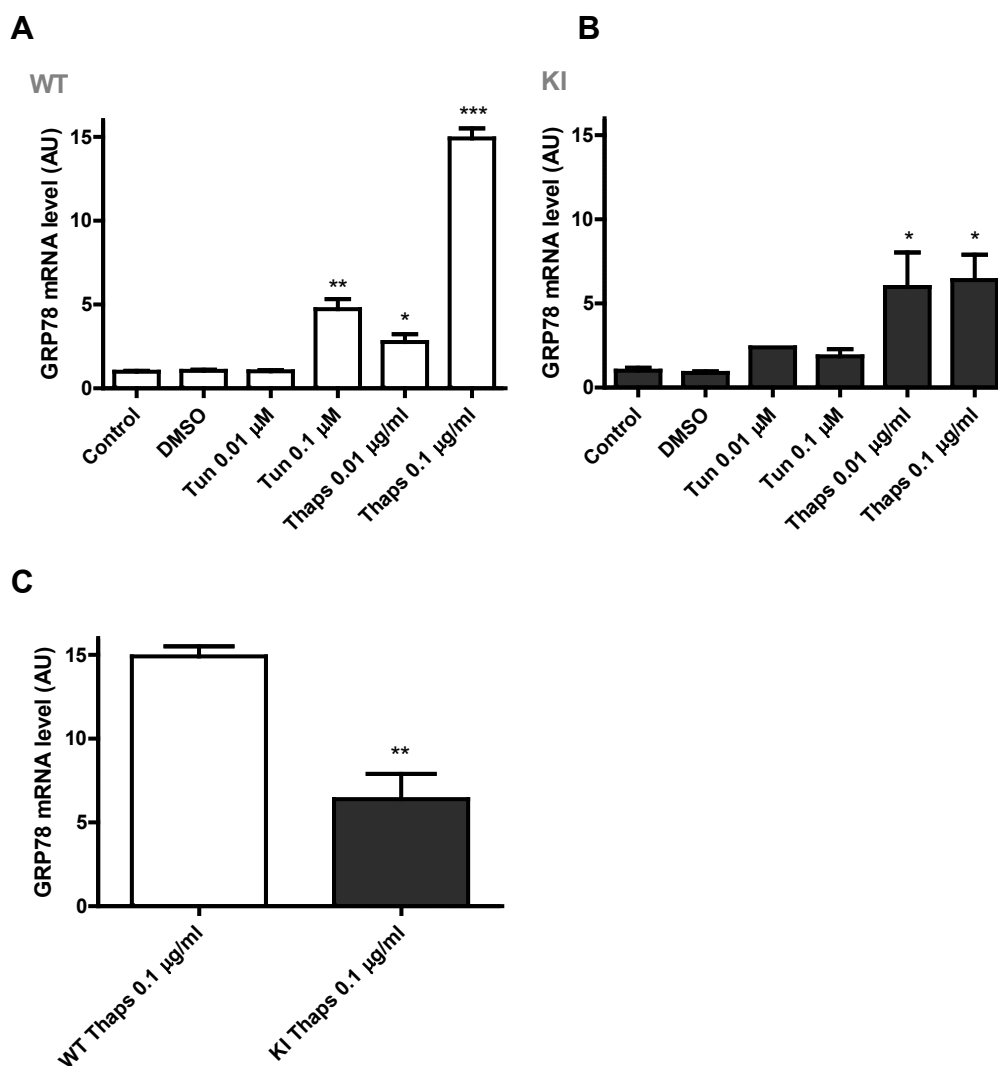


Figure 3.24: Determination of the GRP78 mRNA level in WT (A), KI (B) and WT- vs. KI-NMCM (C). Total RNA was reversed transcribed to cDNA and amplified by quantitative PCR using specific primers. G α S was used as an endogenous control. The number of samples equals 3, except for the KI at tunicamycin 0.1 μ M (n=2). Bars represent the mean \pm SEM with * P <0.05, ** P <0.01 and *** P <0.001 vs. control, Student's t-test.

3.4.2.2 Determination of XBP-1-spliced mRNA levels

The measurement of XBP-1-spliced mRNA revealed comparable results as in 3.4.2.1. In WT-NMCM (Figure 3.25A), at low concentration of tunicamycin no significant effect was detectable. At higher concentration of tunicamycin XBP-1-spliced mRNA was 1.6-fold higher. At low thapsigargin concentration, likewise, no significant effect was measured, whereas a \sim 4-fold higher mRNA level was detected at high concentration than in control

cells. Interestingly, KI-NMCM (Figure 3.25B) reacted very similar to the previous measurement of GRP78. Again, the overall effect was weakened and variation of means was increased compared to WT. By trend, the expression increased depending on the used concentration for both tunicamycin and thapsigargin. At higher concentration thapsigargin treatment revealed a ~ 2.5-fold higher mRNA level. Interestingly, similarly to previous measurements of GRP78, also in this measurement the KI-NMCM reacted with an attenuated increase of spliced XBP-1 mRNA level compared to WT (Figure 3.25C). In conclusion these data support earlier indications of a blunted effect in KI-NMCM.

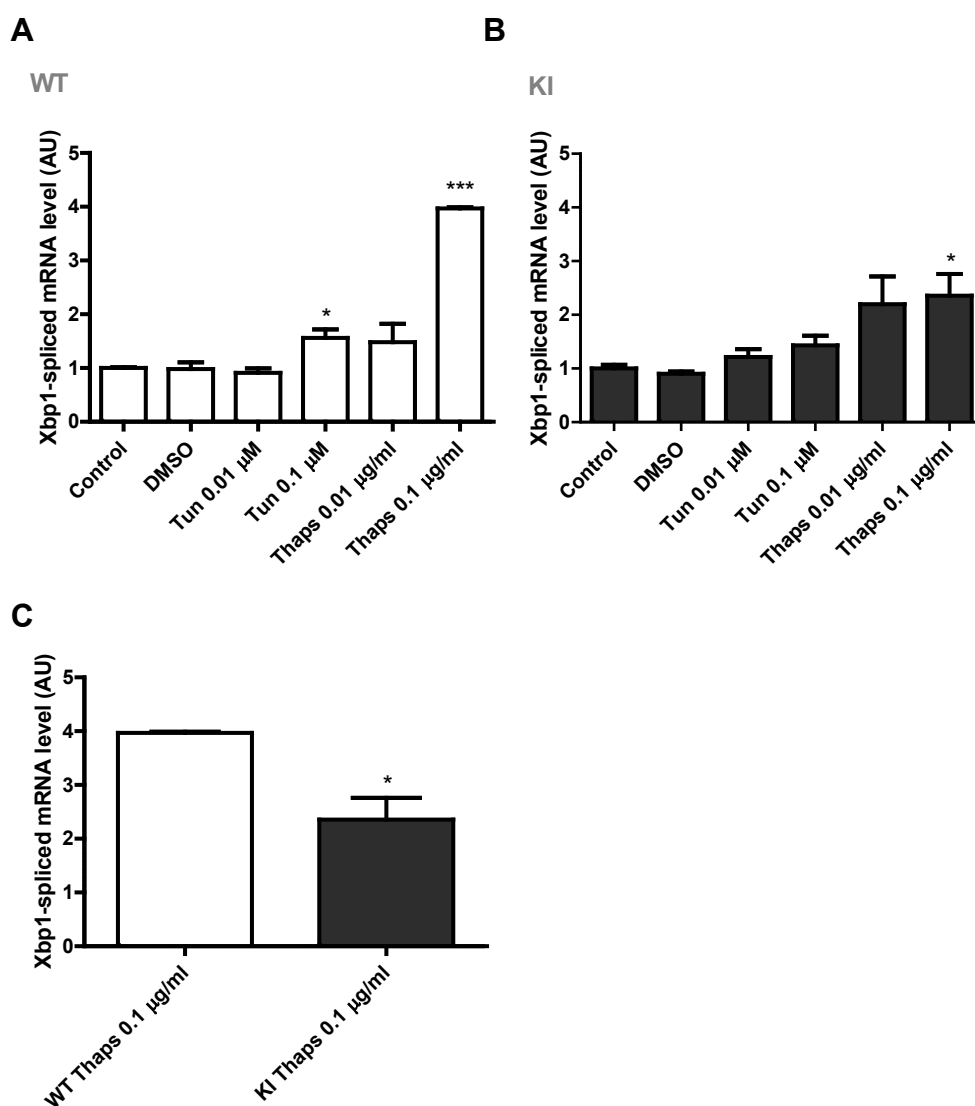


Figure 3.25: Determination of the XBP-1 spliced mRNA level in WT (A), KI (B) and WT- vs. KI-NMCM (C). Total RNA was reversed transcribed to cDNA and amplified by quantitative PCR using specific primers. *GαS* was used as an endogenous control. The number of samples equals 3. Bars represent the mean±SEM with * P <0.05, and *** P <0.001 vs. Control, Student's t-test.

3.4.2.3 Determination of CHOP mRNA levels

CHOP mRNA levels were determined equally as in previous experiments to gain insights into potential apoptotic behavior due to treatment.

Similar to previous results WT-NMCM (Figure 3.26A) reacted as expected with a considerable increase in the CHOP mRNA levels by raising UPR inducers concentrations. At low concentration, tunicamycin effects were mild, while the higher concentration increased ~4-fold the mRNA level of CHOP. Similarly, thapsigargin increased ~1.7-fold CHOP mRNA level at low concentration and ~17-fold at high concentration. Again KI-NMCM (Figure 3.26B) exhibited a very heterogeneous behavior. Though all conditions increased CHOP mRNA level by trend, only cells treated with high concentration of thapsigargin showed significantly 14.2-fold higher CHOP mRNA levels than untreated cells. Interestingly, in contrast to the blunted activation of GRP78 and spliced XBP-1 in KI, CHOP mRNA levels did not differ between KI and WT at high concentration of thapsigargin (Figure 3.26C). This suggests that the KI mutation does not attenuate the ATF6 pathway.

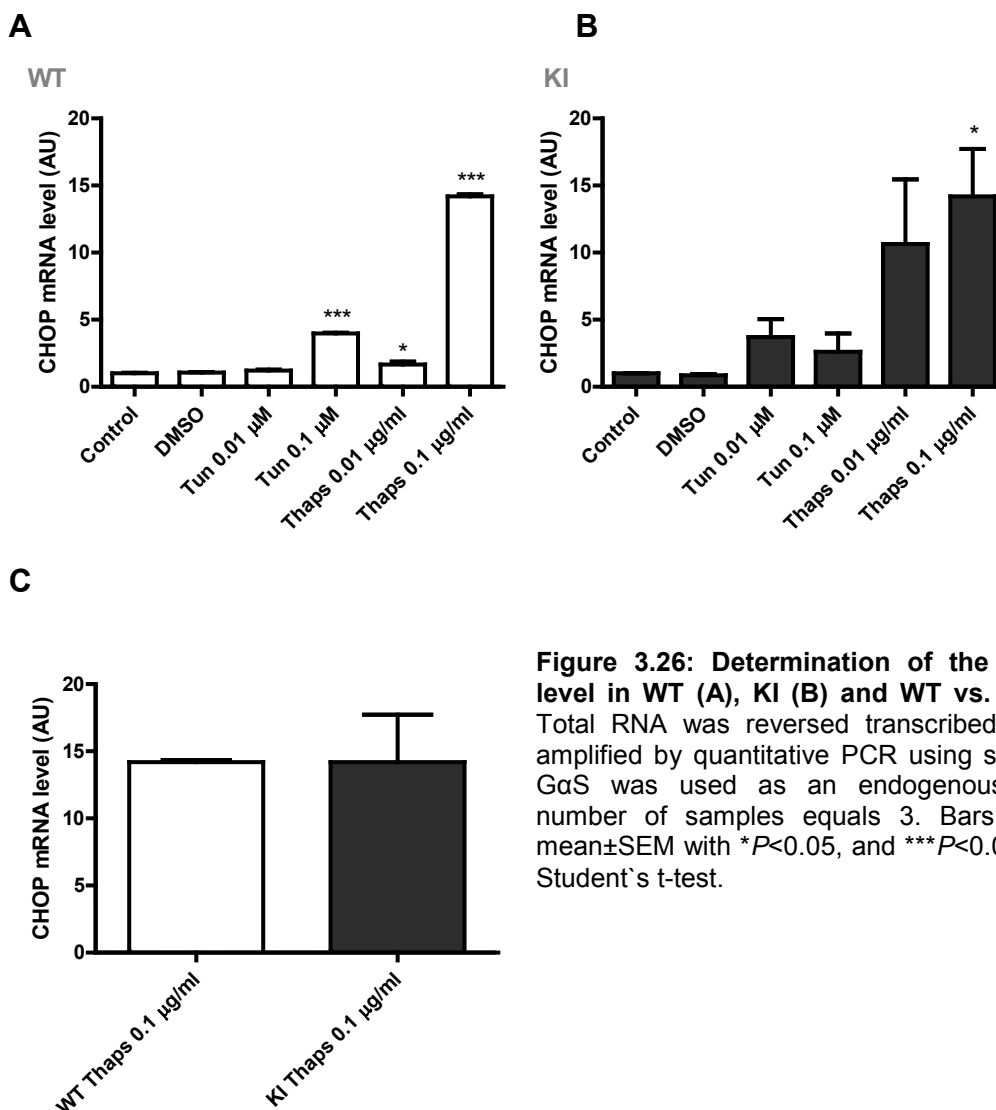


Figure 3.26: Determination of the CHOP mRNA level in WT (A), KI (B) and WT vs. KI NMCM (C). Total RNA was reversed transcribed to cDNA and amplified by quantitative PCR using specific primers. G α S was used as an endogenous control. The number of samples equals 3. Bars represent the mean \pm SEM with * P <0.05, and *** P <0.001 vs. Control, Student's t-test.

3.4.3 Summary

The major findings of this part were the following:

- In contrast to cardiac tissue analysis GRP78 mRNA levels did not differ between KI- and WT-NMCM in basal conditions.
- The mRNA levels of GRP78, spliced XBP-1 and CHOP were markedly higher with the ER stress inducers tunicamycin and thapsigargin in both WT- and KI-NMCM.
- High concentrations of thapsigargin induced a lower activation of GRP78 and spliced XBP-1 in KI- than in WT-NMCM.

These data revealed defective UPR in KI-NMCM with high level of ER stress. Though lower level of GRP78 were revealed, only IRE1 α pathway, but not ATF6 pathway was found to be defective in KI-NMCM.

4 Discussion

An activation of the UPR could be demonstrated in the pathology of heart failure, ischemic heart disease and atherosclerosis (for review, see Minamino et al., 2010). Besides, there is very little knowledge about an involvement of the UPR in HCM. Therefore our intention was to use two different mouse models to investigate the UPR's behavior in reaction to these pathologic conditions. Although both mouse models exhibit LVH and cardiac dysfunction and therefore share almost equal phenotypes, the underlying cause seems to be very different. While the homozygous KO model does not express *Mybpc3*, a low level of mutant cMyBP-C could be detected in the homozygous KI model (Vignier et al., 2009). Therefore we established the conditions to compare a model of pure cMyBP-C insufficiency with a model based on a mutant cMyBP-C. Recognizing previous reports of an impairment of the ubiquitin-proteasome system in rat cardiomyocytes (Sarikas et al., 2005) and accumulation of ubiquitinated proteins in 9-week-old KI mice, we expected impairment of the ubiquitin-proteasome system due to constant degradation of overexpressed mutant cMyBP-C. In response to this impairment, we assumed activation of the UPR in *Mybpc3-targeted* mice.

The major findings of this study were the following:

- The ubiquitin-proteasome system is impaired in one-year-old KI, but not KO mice.
- The UPR (IRE1 α pathway only) is impaired in KI, and activated in KO.
- Pharmacological induction of ER stress results in a blunted UPR in KI-NMCM.

4.1 Impairment of the ubiquitin-proteasome system in *Mybpc3*-KI mice

Determination of the Ub^{G76V}-GFP protein levels allowed evaluating the global function of ubiquitin-proteasome system *in vivo* (Lindsten et al., 2003). The findings of higher Ub^{G76V}-GFP protein levels in one-year-old KI mice suggest inhibition of the ubiquitin-proteasome system, likely due to the constant degradation of mutant cMyBP-C leading to saturation of the system with age. Whereas the chymotrypsin-like activity was not significantly lower in KI compared to WT, it was much lower in KI than in KO. These findings confirm previous reports of impairment of the ubiquitin-proteasome system in rat myocytes overexpressing mutant cMyBP-C (Sarikas et al., 2005) and reduced activities of the proteasome in humans with HCM (Predmore et al., 2010). Due to the genetic setting of the mouse models, it seems reasonable to attribute the impairment in

the KI to mutant cMyBP-C. Whether an impairment of the ubiquitin-proteasome system contributes directly to the pathogenesis of HCM is still subject of many investigations. Recognizing *higher* proteasome activities in 9-week-old KI mice (Vignier et al., 2009), our investigation of a proteasome *impairment* in one-year-old KI mice suggests this dysfunction to appear with age. Therefore the contribution of proteasome impairment to the early pathogenesis seems unlikely, but an influence on pathology with time cannot be ruled out. Accumulation of proteins due to an inhibition of ubiquitin-proteasome system was demonstrated in neurodegenerative diseases such as Alzheimer's (Keller et al., 2000; for review, see Nijholt et al., 2011). Likewise several cases of UPR activations due to accumulating proteins can already be found in the literature. The increased expression of GRP78 and CHOP could be detected in many cases of diseases exhibiting accumulation of proteins, such as Huntington's (Carnemolla et al., 2009), Parkinson's disease or amyotrophic lateral sclerosis (Matus et al., 2011). Acknowledging these reports we hypothesized that our determined impairment of the ubiquitin-proteasome system in KI should cause an activation of the UPR in KI, but not in KO.

4.2 Decreased UPR in *Mybpc3*-KI mice

Trying to determine the activity of the UPR in our mouse models, we investigated many of its pathways' components. Upon activation the UPR upregulates many target genes, such as chaperones or pro-apoptotic factors like CHOP, in order to enhance its folding capacity or initiate apoptosis (Samali et al., 2010). Besides, upon activation the UPR increases levels of its own pathway participants, e.g. spliced XBP-1 (Calfon et al., 2002). Therefore an activation of the UPR is well detectable by measuring mRNA levels by quantitative PCR. In contrast to our hypothesis we disproved UPR activation in the KI mouse model. Classical RT-PCR suggested lower levels of GRP78 mRNA in KI compared to WT mice, which indicated rather impairment than activation of the UPR. These findings were later repeatedly confirmed by RT-qPCR. Also further animals at different ages (neonates and 9-week-old) exhibited significantly lower levels of GRP78 mRNA. Finally, the measurement of lower levels of spliced (activated) XBP-1 mRNA in KI mice indicated an overall decreased activity of the UPR's IRE1 pathway in KI mice.

To further investigate a potential impairment of the IRE1 pathway in KI mice we established another experimental model in cell cultured KI-NMCM, which is receptive for drug treatment. However, first of all GRP78, spliced XBP-1 and CHOP mRNA levels were determined in *untreated* WT- and KI-NMCM in order to reproduce our results of decreased UPR activity in KI mice. Yet, lower mRNA levels of GRP78, spliced XBP-1 or CHOP could

not be detected in untreated KI-NMCM in basal conditions. As potential explanations, the missing interactions of KI-NMCM with other cells (e.g. fibroblasts), generally lower levels of ER stress in cell culture, the controlled medium, as well as a lack of dead cells should be considered. Using thapsigargin and tunicamycin, which are capable to induce additional ER stress, we again evaluated the factors GRP78, spliced XBP-1 and CHOP. Using thapsigargin and tunicamycin, which are capable to induce additional ER stress, a marked increase in the GRP78, spliced XBP-1 and CHOP mRNA levels was found in both WT and KI cardiac myocytes. Most importantly, the increase in GRP78 and spliced XBP-1 mRNA levels with high concentration of thapsigargin was significantly lower in KI cells than in WT. These findings might indicate an alteration of the UPR as it was similarly detected in a different study on Alzheimer's disease by Katayama et al. (2001). Indeed, in this study, tunicamycin-induced UPR was observed at different time points revealing delayed expression of GRP78 due to an attenuated activation of IRE1 in cells expressing mutant presenilin-1. The authors suggested that the lower GRP78 induction may cause increased susceptibility to cellular stresses. Similar hypothesis could be drawn for the KI. In consequence blunted UPR might decrease the cellular capacity to counteract protein accumulation or other cellular stresses in KI cells, as demonstrated in Alzheimer's (Katayama et al., 1999) or diabetes (Harding et al., 2001).

Demonstrated causes of UPR impairment, such as direct inhibition of UPR sensors by mutant proteins (Katayama et al., 1999) should also be considered in the case of mutant cMyBP-C, which suggests direct interaction of mutant cMyBP-C with UPR pathways. An alternative is that the UPR might be attenuated indirectly. The accumulation of hypertrophic or anti-apoptotic factors due to an impairment of the ubiquitin-proteasome systems has been supposed to be relevant for the pathogenesis of HCM (for review, see Mearini et al., 2008). As a consequence of this, also the UPR might be impaired by accumulating factors due to feedback mechanisms. Besides it is necessary to determine whether our detected effects have significant impact on cellular homeostasis at all. Thinkable approaches will be discussed below.

4.3 Increased UPR in *Mybpc3*-KO mice

To better understand the results obtained in KI mice we evaluated the UPR in the KO model. Though the ubiquitin-proteasome system function was not altered in KO mice, higher protein levels of IRE1 α and accordingly increased levels of spliced XBP-1 mRNA rather suggested the pathway's activation. Reports of increased UPR activity in other forms of cardiac hypertrophy support the theory of the UPR initiating adaptive countermeasures (Okada et al., 2004). Therefore, the data obtained in KO model suggest an adaptive UPR activation in cardiac hypertrophy. However, also in this case remaining factors such as CHOP or Bcl-2 were not altered, hereby contradicting an overall activation of the UPR. Since we could not determine a dysfunction of the ubiquitin-proteasome system in the KO mice, other triggers of UPR induction, such as ER protein overload, disturbed calcium homeostasis, oxidative stress, hypoxia and enhanced protein synthesis (for review, see Minamino et al., 2010) should be further evaluated. Since basic investigations on e.g. oxidative stress antagonist Metallothionein-1 did not reveal additional triggers of the UPR, different approaches should be considered. Additionally to the identification of triggers of the UPR in the KO model, it should be investigated whether this different level of UPR activity has impact on cellular homeostasis or even the phenotype. Similar levels of LVH in both models contradict beneficial effects of an increased UPR in KO mice. Yet the general functionality of the UPR in KO was not disproved. Therefore the KO model seems receptive for concepts like intentional UPR manipulation, e.g. overexpression of chaperones to increase ER stress resistance as demonstrated in Alzheimer's (Katayama et al., 1999).

4.4 Impact of UPR alterations on HCM and outlook

Interestingly, despite significant indications for an impairment of the IRE1 pathway in KI mice, the remaining factors of the UPR were rather indifferent. Similarly, analysis of KO mice suggested an activation of the IRE1 pathway only. There are several examples of single pathway activations (for review see Lin et al., 2008), which also seem reasonable considering the individual tasks of the different pathways. An activation of the IRE1 pathway to increase chaperone capacity should precede the activation of the ATF6 pathway, which aims for the initiation of apoptosis. Okada et al. demonstrated increased expression of the UPR-regulated chaperones GRP78 and calreticulin in both hypertrophied and failing hearts after transverse aortic constriction (1 week and 4 weeks with respect to hypertrophy and heart failure, respectively), suggesting UPR

activation (2004). Interestingly, only failing hearts featuring severe lung congestion exhibited higher levels of CHOP, which supports the possibility of single pathway activations. Likewise, the single IRE1 pathway activation in *Mybpc3*-KO mice seems reasonable in order to counteract disturbances due to the detected impairment of the ubiquitin-proteasome system without initiating UPR-dependent apoptosis.

In comparison, impairment of the UPR as detected in *Mybpc3*-KI mice does not seem reasonable with regards to the pathogenesis of HCM, but it seems difficult to determine whether this effect itself is directly pathogenic. While there are many reports of overall UPR activations comparatively little is known about an UPR failure or impairment. Investigations on models of Gaucher's and Niemann-Pick-disease, two lysosomal storage diseases, recently demonstrated unaltered levels of the UPR actors GRP78, XBP-1 and CHOP against expectations (Farfel-Becker et al., 2009; Klein et al., 2011). However, these results suggest an *absence* of UPR not impairment, as it is suggested by decreased levels in *Mybpc3*-KI mice or NCMs. In conclusion Klein et al. expected the UPR to be rather uninvolved in the pathology of Niemann-Pick-disease, while in our study indications for UPR impairment indeed might be relevant to cellular homeostasis. One of the few examples of UPR impairment yet demonstrated the potential drastic consequences. Here UPR failure caused death of the pancreatic beta cells (Harding et al., 2001). In conclusion it seems reasonable to suspect that the determined decreased UPR in KI mice might be adverse to the pathogenesis of HCM, independent from whether it is an adaptive or autonomous mechanism. The given example of a mechanism of direct inhibition of UPR receptors by mutant proteins in Alzheimer's (Katayama et al., 1999) and the results of this investigation suggest potential mechanisms of failure. However, so far, it is not possible to assess whether the detected alterations in *Mybpc3*-KI mice in comparison to WT are signs of physiological reactions or trails of a pathologic mechanism.

Therefore, future investigations should again focus on both models of *Mybpc3*-targeted mice. Concerning the KO model, it seems important to explain the increase in IRE1 pathway activity by identifying further potential triggers. Protein aggregates and ER overload have been identified as a key feature of myocytes in HCM (Maron et al., 1975) and seem to be well detectable in histology. Several antioxidants besides Metallothionein-1 have been shown to be increased in conditions of strong UPR activation (Malhotra et al., 2008) and therefore seem very helpful in order to determine the cellular level of oxidative stress. Regarding the KI model, it might be very helpful to investigate whether there is direct interaction of mutant cMyBP-C with components of the UPR. Physically interaction of presenilin-1 with IRE1 was detected in the previously mentioned study by Katayama et al. using co-immunoprecipitation (1999). This approach might be

adapted to our model of mutant cMyBP-C. Furthermore, the effect of decreased UPR, especially of lower GRP78 levels, should be investigated in human HCM myocardial tissues, since Katayama et al. successfully detected decreased levels of GRP78 in brains of Alzheimer's patients, which validated results of their cell culture experiments (2001).

A very pragmatic approach, which might be evaluated in both KI and KO models, and even might suggest possible treatment perspectives regarding HCM, was demonstrated in diabetes-research. Mihaly et al. detected an improvement of the pathologic features of diabetic retinopathy by the use of the chaperone inducer canavenine (1998). In this study the authors found a modest induction of the chaperone HSP70, yet causing an acceleration of protein turnover. In this way, they suggested that the improved protein degradation might contribute to an improvement in pathology. Following these findings it seems reasonable to consider the induction of chaperones to investigate a potential improvement of UPR activity or even pathologic features in the mouse models of HCM. More precisely, the usage of a chaperone inducer might be able to compensate the lower levels of GRP78 in the KI genotype and reveal its importance for cellular homeostasis. Additional examples for this approach were given in models of Alzheimer's again. Increased resistance to ER stress and protection against neuronal cell death was demonstrated by the infection of cells with a virus expressing recombinant GRP78 (Katayama et al., 1999). Using a different method, Kudo et al. identified BIX (BIP/GRP78 inducer X) in a screening for compounds capable to induce chaperones as an inducer of GRP78, GRP94 and calreticulin. Upon treatment they demonstrated reduced cell death induced by ER stress in neuroblastoma cells (Kudo et al., 2008).

In summary, the forced induction of chaperones in any models of HCM might illuminate the significance of our so far detected effects. Also regarding the ubiquitin-proteasome system increased levels of chaperones might be helpful to decrease competition of its substrates. Hereby further disturbance of the UPR as well as the accumulation of proteins might be attenuated, as already demonstrated in native rat cardiomyocytes (Fu et al., 2008).

4.5 Clinical relevance and concluding remarks

Acknowledging the given examples of demonstrated UPR impacts on pathology, it is interesting to think of UPR impairment as a contributor to HCM's pathogenesis and further investigations of potential mechanisms seem very reasonable. Currently, there are several mechanisms proposed for the pathogenesis of HCM. Besides considering mutant cMyBP-C a "poison polypeptide" or a deficit of physiological cMyBP-C causing functional

haploinsufficiency, it was supposed that there is saturation of the ubiquitin-proteasome system due to the constant degradation of mutant cMyBP-C (for review, see Carrier, 2010). Hereby accumulation of hypertrophic or apoptotic factors might be induced (Mearini et al., 2008). Dysfunction of the UPR in cases of HCM complements the spectrum of theories.

So far, our findings regarding the UPR in HCM point out to the diversity of this cellular mechanism. While in many cases the available data suggest a demand for the attenuation of parts of the UPR as demonstrated by intense apoptosis in heart insufficiency (Okada et al., 2004), our investigation indicates a lack of activation as a potential aim of intervention. In this way these reports reflect the two main targets of research regarding the pharmaceutical manipulation of the UPR. While certain pathways should be enhanced to increase resistance to cellular stress, it seems beneficial to attenuate UPR-mediated apoptosis. Yet, pharmacological intervention is limited by our knowledge about how signaling switches from adaption to cell death (for review, see Minamino et al., 2010).

Targeting the last link of the chain, the induction or even the application of chaperones seems promising, as described earlier. In this manner Ozcan et al. restored glucose homeostasis using the pharmaceutical chaperone 4-phenyl butyric acid in a mouse model of type 2 diabetes (2006). However, also this approach is still very limited because of the high concentrations needed to experience the requested effects in the animal model. Besides, pharmaceuticals interfering within the UPR's pathways, such as a direct CHOP inhibitor are not yet available (for review, see Minamino et al., 2010).

In conclusion, it seems important to improve our knowledge of the functionality of the UPR in physiology and pathology. Hereby, additional understanding of the pathogenesis of cardiovascular disease and many others might lead to new therapeutic strategies. Especially in the case of HCM further investigations might be very promising due to the so far detected mechanisms and their potential proximity to pathology.

5 Abstract

Familial hypertrophic cardiomyopathy (HCM) is a common (1:500) inherited cardiac disorder. It is mainly characterized by left ventricular hypertrophy and increased interstitial fibrosis. The individual patient's clinical course varies from sudden cardiac death during adolescence to chronic heart failure in old age. In approximately one third of all cases, HCM is caused by mutations in the *Mybpc3* gene encoding cardiac myosin-binding protein C (cMyBP-C). Recently, interference of mutant cMyBP-C with the ubiquitin-proteasome system, which is responsible for the degradation of the majority of cellular proteins, was demonstrated. Disturbances within the cellular protein homeostasis are major triggers of the unfolded protein response (UPR), a key feature of cellular protein accumulation reactions. The UPR consists of a set of three pathways (IRE1, ATF6 and PERK), each monitoring the conditions within the lumen of the endoplasmic reticulum (ER). In case of ER stress these pathways initiate different counter measures of which are most important: (1) Increase of chaperone expression (mostly IRE1); (2) Decrease of protein synthesis (mostly PERK) and (3) apoptosis (ATF6) in case of failure of (1) and (2). This investigation focused on an expected activation of the UPR in models of HCM due to mutations in *Mybpc3*. The first HCM mouse model (KI) carries a point mutation and exhibits low levels of mutant cMyBP-C, while the second model is a homozygous *Mybpc3*-knock-out (KO) and serves as a model of cMyBP-C insufficiency. Both models were crossed to the Ub^{G76V}-GFP mice, which report the activity of the proteasome. Furthermore, investigations were performed in KI-neonatal mouse cardiomyocytes (KI-NMCM) which are receptive to drug treatment. Fundamental parameters were determined on mRNA and/or protein levels to evaluate overall and single pathway activities of the UPR. Higher protein levels of Ub^{G76V}-GFP in 1 year-old KI, but not KO than in WT suggest impairment of the ubiquitin-proteasome system. Interestingly lower or unaffected mRNA levels of multiple UPR parameters (IRE1, GRP78, XBP-1) suggest *decreased* activity of the UPR in KI model in contrast to our hypothesis. In comparison, the analysis of the KO model revealed increased expression within the IRE1 pathway, suggesting at least partial activation of the UPR. The decreased UPR activity and hereby a potential defect, could not be reproduced in NMCM in basal condition. However treatment with high concentration of the UPR inducing drug thapsigargin revealed an attenuated response in KI- compared to WT-NMCM. These data suggest a decreased activity of the UPR in the KI mouse model, which should be investigated further. Disturbances of the UPR have been identified as causes of pathology in neurodegenerative and diabetic diseases. Therefore this approach might have promising relevance to the investigation of the pathogenesis of HCM.

6 Deutsche Zusammenfassung

Familiäre hypertrophe Cardiomyopathie (HCM) ist eine häufige (1:500) erbliche Herzkrankheit. Sie ist gekennzeichnet durch linksventrikuläre und interstitielle Fibrose. Der individuelle Krankheitsverlauf reicht vom plötzlichen Herztod in der Jugend bis zur chronischen Herzinsuffizienz in hohem Alter. In ca. einem Drittel der Fälle wird HCM verursacht durch Mutationen im *Mybpc3* Gen, welches das cardiac myosin-binding protein C (cMyBP-C) kodiert. Kürzlich wurde die Interferenz von mutiertem cMyBP-C mit dem Ubiquitin-Proteasom-System nachgewiesen. Dieses ist für den Abbau des Großteils zellulärer Proteine verantwortlich. Störungen dieses Abbaus sind ein Hauptauslöser der unfolded protein response (UPR), ein wichtiger Abwehrmechanismus zellulärer Proteinakkumulation. Die UPR besteht aus drei Signalwegen (IRE1, ATF6 und PERK), welche das Innere des Endoplasmatischen Retikulums überwachen. Im Falle einer Störung leiten die Signalwege unterschiedliche Gegenmaßnahmen ein, von denen die wichtigsten sind: (1) Steigerung der Chaperon Expression (v.a. IRE1); (2) Reduzierung der Proteinsynthese (v.a. PERK) und (3) Apoptose, falls (1) und (2) fehlschlagen. Auf dieser Grundlage überprüft diese Arbeit eine erwartete Aktivierung der UPR in Modellen der HCM auf der Basis von Mutationen in *Mybpc3*. Das erste dieser Modelle trägt eine Punktmutation und zeigt geringe Konzentrationen mutierten C-Proteins. Das zweite dient als homozygoter *Mybpc3* knock-out (KO) als Model der cMyBP-C-Insuffizienz. Desweiteren wurden neonatale Rattencardiomyocyten zum Vergleich und zur pharmakologischen Intervention genutzt. Fundmentale Parameter wurden dann auf mRNA- und/oder Proteinebene bestimmt, um die Aktivität der UPR zu analysieren. Erhöhte Proteinwerte von Ub^{G76V}-GFP in ein Jahr alten KI, aber nicht in KO deuten auf eine Beeinträchtigung des ubiquitin-proteasome systems hin. Entgegen unserer Erwartungen zeigte sich jedoch eine erniedrigte oder unveränderte Expression wichtiger UPR Parameter (IRE1, GRP78, XBP-1), die auf eine abgeschwächte Aktivität der UPR im KI Model hindeutet. Im Vergleich ergab die Analyse des KO Modells Hinweise auf eine teilweise Aktivierung der UPR im IRE1 Signalweg. Die eingeschränkte UPR-Aktivität des KI Modells, die auf einen etwaigen Defekt hinweisen könnte, konnte jedoch nicht im unbehandelten NMCM Modell reproduziert werden. Interessanterweise zeigte sich jedoch während der Behandlung mit dem UPR Induktor Thapsigargin eine abgeschwächte UPR der KI- im Vergleich zu WT-NMCM. Die geschilderten Ergebnisse geben Hinweise auf eine eingeschränkte Aktivität der UPR im KI Mausmodell. Störungen der UPR Aktivität konnten bereits als Ursache neurodegenerativer und diabetischer Erkrankungen identifiziert werden. Vor diesem Hintergrund könnten die Erkenntnisse dieser Arbeit vielversprechende Bedeutung für die Entwicklung der HCM haben.

7 Literature

Bear, M. F. C., Barry W.; Paradiso, Michael A. (2006). Neuroscience, Exploring the Brain. Philadelphia, Lippincott Williams & Wilkins.

Bell, S. G. and B. L. Vallee (2009). "The metallothionein/thionein system: an oxidoreductive metabolic zinc link." *Chembiochem* 10: 55-62.

Bertolotti, A., Y. Zhang, et al. (2000). "Dynamic interaction of BiP and ER stress transducers in the unfolded-protein response." *Nat Cell Biol* 2: 326-332.

Bonne, G., L. Carrier, et al. (1998). "Familial hypertrophic cardiomyopathy: from mutations to functional defects." *Circ Res* 83: 580-593.

Buchou, T., M. Vernet, et al. (2003). "Disruption of the regulatory beta subunit of protein kinase CK2 in mice leads to a cell-autonomous defect and early embryonic lethality." *Mol Cell Biol* 23: 908-915.

Calfon, M., H. Zeng, et al. (2002). "IRE1 couples endoplasmic reticulum load to secretory capacity by processing the XBP-1 mRNA." *Nature* 415: 92-96.

Carnemolla, A., E. Fossale, et al. (2009). "Rrs1 is involved in endoplasmic reticulum stress response in Huntington disease." *J Biol Chem* 284: 18167-18173.

Carrier, L. (2010). "Too much of a good thing is bad: proteasome inhibition induces stressed hearts to fail." *Cardiovasc Res* 88: 389-390.

Carrier, L., G. Bonne, et al. (1997). "Organization and sequence of human cardiac myosin binding protein C gene (MYBPC3) and identification of mutations predicted to produce truncated proteins in familial hypertrophic cardiomyopathy." *Circ Res* 80: 427-434.

Carrier, L., R. Knoll, et al. (2004). "Asymmetric septal hypertrophy in heterozygous cMyBP-C null mice." *Cardiovasc Res* 63: 293-304.

Cuello, F., S. C. Bardswell, et al. (2011). "Novel role for p90 ribosomal S6 kinase in the regulation of cardiac myofilament phosphorylation." *J Biol Chem* 286: 5300-5310.

Dahlmann, B. (2007). "Role of proteasomes in disease." *BMC Biochem* 8 Suppl 1: S3.

Delepine, M., M. Nicolino, et al. (2000). "EIF2AK3, encoding translation initiation factor 2-alpha kinase 3, is mutated in patients with Wolcott-Rallison syndrome." *Nat Genet* 25: 406-409.

Farfel-Becker, T., E. Vitner, et al. (2009). "No evidence for activation of the unfolded protein response in neuronopathic models of Gaucher disease." *Hum Mol Genet* 18: 1482-1488.

Fu, H. Y., T. Minamino, et al. (2008). "Overexpression of endoplasmic reticulum-resident chaperone attenuates cardiomyocyte death induced by proteasome inhibition." *Cardiovasc Res* 79: 600-610.

- Fu, H. Y., K. Okada, et al. (2010). "Ablation of C/EBP homologous protein attenuates endoplasmic reticulum-mediated apoptosis and cardiac dysfunction induced by pressure overload." *Circulation* 122: 361-369.
- Galehdar, Z., P. Swan, et al. (2010). "Neuronal apoptosis induced by endoplasmic reticulum stress is regulated by ATF4-CHOP-mediated induction of the Bcl-2 homology 3-only member PUMA." *J Neurosci* 30: 16938-16948.
- Harding, H. P., H. Zeng, et al. (2001). "Diabetes mellitus and exocrine pancreatic dysfunction in *perk*^{-/-} mice reveals a role for translational control in secretory cell survival." *Mol Cell* 7: 1153-1163.
- Harris, J. L., P. B. Alper, et al. (2001). "Substrate specificity of the human proteasome." *Chem Biol* 8: 1131-1141.
- Iwata, Y. and N. Koizumi (2005). "Unfolded protein response followed by induction of cell death in cultured tobacco cells treated with tunicamycin." *Planta* 220: 804-807.
- Katayama, T., K. Imaizumi, et al. (2001). "Disturbed activation of endoplasmic reticulum stress transducers by familial Alzheimer's disease-linked presenilin-1 mutations." *J Biol Chem* 276: 43446-43454.
- Katayama, T., K. Imaizumi, et al. (1999). "Presenilin-1 mutations downregulate the signalling pathway of the unfolded-protein response." *Nat Cell Biol* 1: 479-485.
- Kaushal, S. and H. G. Khorana (1994). "Structure and function in rhodopsin. 7. Point mutations associated with autosomal dominant retinitis pigmentosa." *Biochemistry* 33: 6121-6128.
- Keller, J. N., K. B. Hanni, et al. (2000). "Impaired proteasome function in Alzheimer's disease." *J Neurochem* 75: 436-439.
- Kitakaze, M. and O. Tsukamoto (2010). "What is the role of ER stress in the heart? Introduction and series overview." *Circ Res* 107: 15-18.
- Klein, A., M. Mosqueira, et al. (2011). "Lack of activation of the unfolded protein response in mouse and cellular models of niemann-pick type C disease." *Neurodegener Dis* 8: 124-128.
- Kozutsumi, Y., M. Segal, et al. (1988). "The presence of malfolded proteins in the endoplasmic reticulum signals the induction of glucose-regulated proteins." *Nature* 332: 462-464.
- Kudo, T., S. Kanemoto, et al. (2008). "A molecular chaperone inducer protects neurons from ER stress." *Cell Death Differ* 15: 364-375.
- Laugwitz, K. L., A. Moretti, et al. (2005). "Postnatal *Isl1*⁺ cardioblasts enter fully differentiated cardiomyocyte lineages." *Nature* 433: 647-653.
- Lin, J. H., P. Walter, et al. (2008). "Endoplasmic reticulum stress in disease pathogenesis." *Annu Rev Pathol* 3: 399-425.
- Lindsten, K., V. Menendez-Benito, et al. (2003). "A transgenic mouse model of the ubiquitin/proteasome system." *Nat Biotechnol* 21: 897-902.

- Ludwig, A., B. Friedel, et al. (2005). "Effect of statins on the proteasomal activity in mammalian endothelial and vascular smooth muscle cells." *Biochem Pharmacol* 70: 520-526.
- Ma, Y. and L. M. Hendershot (2003). "Delineation of a negative feedback regulatory loop that controls protein translation during endoplasmic reticulum stress." *J Biol Chem* 278: 34864-34873.
- Magne, L., E. Blanc, et al. (2011). "ATF4 and the integrated stress response are induced by ethanol and cytochrome P450 2E1 in human hepatocytes." *J Hepatol* 54: 729-737.
- Malhotra, J. D., H. Miao, et al. (2008). "Antioxidants reduce endoplasmic reticulum stress and improve protein secretion." *Proc Natl Acad Sci U S A* 105: 18525-18530.
- Maquat, L. E. (2005). "Nonsense-mediated mRNA decay in mammals." *J Cell Sci* 118: 1773-1776.
- Maron, B. J. (2002). "Hypertrophic cardiomyopathy: practical steps for preventing sudden death." *Phys Sportsmed* 30: 19-24.
- Maron, B. J., V. J. Ferrans, et al. (1975). "Ultrastructural features of degenerated cardiac muscle cells in patients with cardiac hypertrophy." *Am J Pathol* 79: 387-434.
- Maron, B. J., J. M. Gardin, et al. (1995). "Prevalence of hypertrophic cardiomyopathy in a general population of young adults. Echocardiographic analysis of 4111 subjects in the CARDIA Study. Coronary Artery Risk Development in (Young) Adults." *Circulation* 92: 785-789.
- Maron, B. J., P. F. Nichols, 3rd, et al. (1984). "Patterns of inheritance in hypertrophic cardiomyopathy: assessment by M-mode and two-dimensional echocardiography." *Am J Cardiol* 53: 1087-1094.
- Maron, B. J., J. Shirani, et al. (1996). "Sudden death in young competitive athletes. Clinical, demographic, and pathological profiles." *JAMA* 276: 199-204.
- Matus, S., L. H. Glimcher, et al. (2011). "Protein folding stress in neurodegenerative diseases: a glimpse into the ER." *Curr Opin Cell Biol* 23: 239-252.
- Mearini, G., S. Schlossarek, et al. (2008). "The ubiquitin-proteasome system in cardiac dysfunction." *Biochim Biophys Acta* 1782: 749-763.
- Mihaly, K., S. Toth, et al. (1998). "Attenuation of diabetic retinopathy by the molecular chaperone-inducer amino acid analogue canavanine in streptozotocin-diabetic rats." *Cell Mol Life Sci* 54: 1154-1160.
- Minamino, T. and M. Kitakaze (2010). "ER stress in cardiovascular disease." *J Mol Cell Cardiol* 48: 1105-1110.
- Minamino, T., I. Komuro, et al. (2010). "Endoplasmic reticulum stress as a therapeutic target in cardiovascular disease." *Circ Res* 107: 1071-1082.
- Moolman, J. A., S. Reith, et al. (2000). "A newly created splice donor site in exon 25 of the MyBP-C gene is responsible for inherited hypertrophic cardiomyopathy with incomplete disease penetrance." *Circulation* 101: 1396-1402.

- Nijholt, D. A., L. De Kimpe, et al. (2011). "Removing protein aggregates: the role of proteolysis in neurodegeneration." *Curr Med Chem* 18: 2459-2476.
- Offer, G., C. Moos, et al. (1973). "A new protein of the thick filaments of vertebrate skeletal myofibrils. Extractions, purification and characterization." *J Mol Biol* 74: 653-676.
- Okada, K., T. Minamino, et al. (2004). "Prolonged endoplasmic reticulum stress in hypertrophic and failing heart after aortic constriction: possible contribution of endoplasmic reticulum stress to cardiac myocyte apoptosis." *Circulation* 110: 705-712.
- Ozcan, U., E. Yilmaz, et al. (2006). "Chemical chaperones reduce ER stress and restore glucose homeostasis in a mouse model of type 2 diabetes." *Science* 313: 1137-1140.
- Pohlmann, L., I. Kroger, et al. (2007). "Cardiac myosin-binding protein C is required for complete relaxation in intact myocytes." *Circ Res* 101: 928-938.
- Predmore, J. M., P. Wang, et al. (2010). "Ubiquitin proteasome dysfunction in human hypertrophic and dilated cardiomyopathies." *Circulation* 121: 997-1004.
- Rogers, T. B., G. Inesi, et al. (1995). "Use of thapsigargin to study Ca²⁺ homeostasis in cardiac cells." *Biosci Rep* 15: 341-349.
- Ron, D. and P. Walter (2007). "Signal integration in the endoplasmic reticulum unfolded protein response." *Nat Rev Mol Cell Biol* 8: 519-529.
- Rottbauer, W., M. Gautel, et al. (1997). "Novel splice donor site mutation in the cardiac myosin-binding protein-C gene in familial hypertrophic cardiomyopathy. Characterization Of cardiac transcript and protein." *J Clin Invest* 100: 475-482.
- Ryoo, H. D., P. M. Domingos, et al. (2007). "Unfolded protein response in a Drosophila model for retinal degeneration." *EMBO J* 26: 242-252.
- Sadayappan, S., J. Gulick, et al. (2005). "Cardiac myosin-binding protein-C phosphorylation and cardiac function." *Circ Res* 97: 1156-1163.
- Samali, A., U. Fitzgerald, et al. (2010). "Methods for monitoring endoplasmic reticulum stress and the unfolded protein response." *Int J Cell Biol* 2010: 830307.
- Sarikas, A., L. Carrier, et al. (2005). "Impairment of the ubiquitin-proteasome system by truncated cardiac myosin binding protein C mutants." *Cardiovasc Res* 66: 33-44.
- Schlossarek, S., G. Mearini, et al. (2011). "Cardiac myosin-binding protein C in hypertrophic cardiomyopathy: Mechanisms and therapeutic opportunities." *J Mol Cell Cardiol* 50: 613-620.
- Scirica, B. M. and D. A. Morrow (2004). "Troponins in acute coronary syndromes." *Prog Cardiovasc Dis* 47: 177-188.
- Seidman, J. G. and C. Seidman (2001). "The genetic basis for cardiomyopathy: from mutation identification to mechanistic paradigms." *Cell* 104: 557-567.
- Sherrid, M. V. (2006). "Pathophysiology and treatment of hypertrophic cardiomyopathy." *Prog Cardiovasc Dis* 49: 123-151.

Shintani, K., D. L. Shechtman, et al. (2009). "Review and update: current treatment trends for patients with retinitis pigmentosa." *Optometry* 80: 384-401.

Teare, D. (1958). "Asymmetrical hypertrophy of the heart in young adults." *Br Heart J* 20: 1-8.

Tirasophon, W., A. A. Welihinda, et al. (1998). "A stress response pathway from the endoplasmic reticulum to the nucleus requires a novel bifunctional protein kinase/endoribonuclease (Ire1p) in mammalian cells." *Genes Dev* 12: 1812-1824.

Toko, H., H. Takahashi, et al. (2010). "ATF6 is important under both pathological and physiological states in the heart." *J Mol Cell Cardiol* 49: 113-120.

Tsukamoto, O., T. Minamino, et al. (2010). "Functional alterations of cardiac proteasomes under physiological and pathological conditions." *Cardiovasc Res* 85: 339-346.

Vidal, F., J. Sage, et al. (1998). "Cre expression in primary spermatocytes: a tool for genetic engineering of the germ line." *Mol Reprod Dev* 51: 274-280.

Vignier, N., S. Schlossarek, et al. (2009). "Nonsense-mediated mRNA decay and ubiquitin-proteasome system regulate cardiac myosin-binding protein C mutant levels in cardiomyopathic mice." *Circ Res* 105: 239-248.

Winegrad, S. (1999). "Cardiac myosin binding protein C." *Circ Res* 84: 1117-1126.

8 Appendix

8.1 List of abbreviations

A	Ampere
ADP	Adenosine diphosphate
AMC	7-Amino-4-methylcoumarin
APS	Ammonium persulphate
ATF4	Activating transcription factor 4
ATF6	Activating transcription factor 6
ATP	Adenosine triphosphate
AU	Arbitrary unit
bp	Base pair(s)
Bcl-2	B-cell lymphoma 2 family protein
BSA	Bovine serum albumin
BW	Body weight
°C	Degree Celsius
cDNA	Complementary deoxyribonucleic acid
C _t	Threshold Cycle
cTnI	Cardiac Troponin I
Da	Dalton
DMEM	Dulbecco's Modified Eagle's Medium
DMSO	Dimethyl sulfoxide
DNA	Deoxyribonucleic acid
dNTP	Deoxynucleoside triphosphate
DTT	Dithiothreitol
ECL	Enhanced chemiluminescence
EDTA	Ethylene diamine tetraacetic acid
e.g.	<i>exempli gratia</i> (for example)
EGFP	Enhanced green fluorescent protein
Eif2 α	Eukaryotic translation initiation factor 2 α
ER	Endoplasmic reticulum
ERAD	ER-associated protein degradation
ES	Embryonic stem
<i>et al.</i>	<i>et alii</i> (and others)
FAM	Carboxyfluorescein

FCS	Foetal calf serum
HCM	Familial hypertrophic cardiomyopathy
g	Gram
GAPDH	Glyceraldehyde 3-Phosphate Dehydrogenase
GFP	Green fluorescent protein
GRP78	Glucose related protein 78
h	Hour
HBSS	Hank's Balanced Salt Solution
HCM	Hypertrophic cardiomyopathy
HEPES	4-(2-Hydroxyethyl)-1-piperazineethanesulfonic acid
HW	Heart weight
HECT	Homologous to the E6-AP Carboxyl Terminus
Het	Heterozygous
HSV	Herpes simplex virus
Hz	Hertz
i.e.	<i>id est</i> (that is)
IgG	Immunoglobulin G
Inc.	Incorporation
IRE1 α	Inositol-requiring enzyme 1 α
kb	Kilobase
kDa	Kilo Dalton
KO	knock-out
l	Liter
m	Milli- (1×10^{-3})
M	Molar
mA	Milliampere
Maldi	
mg	Milligram
min	Minutes
ml	Milliliter
mM	Millimolar
μ g	Microgram
μ l	Microliter
μ M	Micromolar
MOI	Multiplicity of infection
MW	Molecular weight
mRNA	Messenger ribonucleic acid

MuRF	Muscle-specific RING-finger
MyBP-C	Myosin-binding protein-C
c MyBP-C	Cardiac Myosin-binding protein-C
μ	Micro (1 x 10 ⁻⁶)
N	Amino-
NaF	Sodium fluoride
NaOH	Sodium hydroxide
NCBI	National Center for Biotechnology Information
NIH	National Institutes of Health
nm	Nanometer
nM	Nanomolar
NMCM	Neonatal mouse cardiomyocytes
no.	Number
oligo(dT)	Oligodeoxythymidylic acid
P	Probability
PAGE	Polyacrylamide gel electrophoresis
PBS	Phosphate buffered saline
PCR	Polymerase chain reaction
PERK	PK-like ER kinase
PS1	Presenelin-1
PVDF	Polyvinylidenedifluoride
RBCC	RING Finger-B-box-coiled-coil
RING	Really Interesting New Gene
RFU	Relative fluorescence unit
RNA	Ribonucleic acid
rpm	Rotation per minute
rRNA	Ribosomal ribonucleic acid
RT	Room temperature
RT-PCR	Reverse transcriptase-PCR
S	Svedberg
SDS	Sodium dodecyl sulfate
sec	Seconds
SEM	Standard error of mean
Suc	Succinyl
sk. m.	Skeletal muscle
TAE	Tris acetate EDTA
TAMRA	Tetramethylrhodamine

TBE	Tris borate EDTA
TBS	Tris buffered saline
TBS-T	Tris buffered saline with tween-20
TEMED	N, N, N', N'-Tetramethylethylenediamine
UPR	Unfolded protein response
UPS	Ubiquitin proteasome system
XBP-1	Xbox-binding protein 1

8.2 Curriculum vitae

Personal Data

Name	Markus Sauer
Date of Birth	22 nd of March 1986
Place of Birth	Kassel, Germany
Nationality	German

Education

1992 - 1996	Elementary School am Heideweg Kassel
1996 - 2005	Abitur Wilhelmshgymnasium Kassel
10/01/2005	Medical School UKE Hamburg
09/17/2008	1 st Medical Examination

Scientific Work

04/2010 - 07/2011	Dissertation Institute of Experimental Pharmacology and Toxicology Hamburg
05/29/2011	Lecture at the 77 th Annual Meeting of the German Cardiac Society

Medical Work

05/2011 - 06/2011	Medical Clerkship - Clinica de Traumatología, Hospital Universitario Salamanca
09/2010 - 10/2010	Medical Clerkship - Ambulant Cardiology Center Kassel
07/2009 - 08/2009	Medical Clerkship - St. Johns Medical Center, Munster, Indiana, USA

8.3 Declaration

I declare that the work reported in this dissertation submitted to the University of Hamburg and entitled

The unfolded protein response in *Mybpc3*-targeted mice with hypertrophic cardiomyopathy

was realized in person in the Institute of Experimental Pharmacology and Toxicology under the supervision of Prof. Dr. Lucie Carrier. All sources of information as well as the results obtained in collaboration with other people are pointed out.

The dissertation has not been submitted in whole or in part for a degree at any other university.

Hamburg, 27 July 2011

Markus Sauer

8.4 Acknowledgement

I would like to thank Prof. Dr. Lucie Carrier for her kind and patient supervision of this thesis. Her enduring encouragement and imperturbable patience in times of work and failure were indispensable contributions to this work.

My sincere gratitude also goes especially to Dr. Saskia Schlossarek. Besides teaching me all methods and answering my countless repeated questions, I am very grateful for her kind personal support during all my time at the institute and especially at the annual meeting in Mannheim.

I thank Prof. Dr. Eschenhagen for his friendly support and his commitment in improving my work and my presentations on many occasions.

Last but not least, I would like to thank all members of the pharmacology department for always being kind and supportive. I felt privileged to work at an institute where everybody is happy to offer his help and personal interest to me and my work.